TKK Dissertations 90
Espoo 2007

STUDIES ON THE DIRECT METHANOL FUEL CELL: CHARACTERIZATION OF PROTON CONDUCTING POLYMER MEMBRANES AND INVESTIGATIONS OF CURRENT DISTRIBUTION AT THE CATHODE

Doctoral Dissertation

Ville Saarinen

Helsinki University of Technology
Department of Chemical Technology
Laboratory of Physical Chemistry and Electrochemistry

TKK Dissertations 90
Espoo 2007

STUDIES ON THE DIRECT METHANOL FUEL CELL: CHARACTERIZATION OF PROTON CONDUCTING POLYMER MEMBRANES AND INVESTIGATIONS OF CURRENT DISTRIBUTION AT THE CATHODE

Doctoral Dissertation

Ville Saarinen

Dissertation for the degree of Doctor of Science in Technology to be presented with due permission of the Department of Chemical Technology for public examination and debate in Auditorium AS1 at Helsinki University of Technology (Espoo, Finland) on the 16th of November, 2007, at 1 p.m.

Helsinki University of Technology
Department of Chemical Technology
Laboratory of Physical Chemistry and Electrochemistry

Teknillinen korkeakoulu
Kemian tekniikan osasto
Fysikaalisen kemian ja sähkökemian laboratorio

Distribution:
Helsinki University of Technology
Department of Chemical Technology
Laboratory of Physical Chemistry and Electrochemistry
P.O. Box 6100
FI - 02015 TKK
FINLAND
URL: http://www.tkk.fi/Units/PhysicalChemistry/
Tel. +358-9-451 2572
Fax +358-9-451 2580
E-mail: vss@cc.hut.fi

© 2007 Ville Saarinen

ISBN 978-951-22-8980-6
ISBN 978-951-22-8981-3 (PDF)
ISSN 1795-2239
ISSN 1795-4584 (PDF)
URL: http://lib.tkk.fi/Diss/2007/isbn9789512289813/

TKK-DISS-2350

Multiprint Oy
Espoo 2007

HELSINKI UNIVERSITY OF TECHNOLOGY
P. O. BOX 1000, FI-02015 TKK
http://www.tkk.fi

ABSTRACT OF DOCTORAL DISSERTATION

Author Ville Sakari Saarinen

Name of the dissertation

STUDIES ON THE DIRECT METHANOL FUEL CELL: CHARACTERIZATION OF PROTON CONDUCTING POLYMER MEMBRANES AND INVESTIGATIONS OF CURRENT DISTRIBUTION AT THE CATHODE

Date of manuscript 2007-05-22 | Date of the dissertation 2007-11-16

☐ Monograph ☒ Article dissertation (summary + original articles)

Department Chemical Technology
Laboratory Physical Chemistry and Electrochemistry
Field of research Fuel Cells
Opponent(s) Professor Göran Lindbergh
Supervisor Professor Kyösti Kontturi
(Instructor) D.Sc. Tanja Kallio

Abstract

Novel proton conducting membranes for the direct methanol fuel cell (DMFC) are characterized widely by combining methods of physical chemistry, electrochemistry and material science. This work mainly concentrates on the sulphonated poly(ethylene-*alt*-tetrafluoroethylene) (ETFE-SA) membrane. Other investigated membranes are poly(vinylidene fluoride)-*graft*-poly(styrene sulphonic acid) (PVDF-*g*-PSSA), sulphonated poly(phenylene sulphone) (sPSO2) and the commercial Nafion® membrane as a reference material. The swelling properties of the membranes are investigated in different alcohol - water and H_2SO_4 - water mixtures. Clear trends are observed for the water / alcohol selectivity: preferential water uptake (alcohol rejection) correlates with high ion exchange capacity (IEC) and low solvent uptake (swelling). The total swelling significantly decreases in the presence of H_2SO_4 indicating that osmosis is a major driving force in the swelling process. The membrane properties are characterized with sophisticated microscopic techniques (AFM, SEM & EDX, SECM) and many benefits of the extensive characterization are demonstrated. The surface hydrophobicity is investigated by water contact angle (CA) measurement. During the measurements, the surface properties of the different membranes are found to differ significantly from each other and the properties of the ETFE-SA membrane to vary also as a function of the manufacturing parameters. Also, the ETFE-SA membrane has exceptionally low water uptake, high water selectivity against methanol and good chemical and mechanical stability. Methanol permeability through the membranes is investigated both with a diffusion cell and under actual DMFC conditions. The membranes are investigated in a laboratory-scale DMFC system and the connections between different operation parameters are clarified in detail. The main observation is that durability of ETFE-SA is sufficient for DMFC applications at low temperatures ($T < 80\ ^\circ C$), as over 2 000 h DMFC testing was carried out without any loss of performance. The methanol crossover and other mass transfer phenomena have been investigated in a free-breathing DMFC both experimentally and computationally. The information on local concentrations of the reacting species is obtained by measuring the current distribution profile using a resistor network approach and a segmented cathode. The developed numerical 3D model describes the behaviour of the free-breathing DMFC and gives spatial information on mass transfer phenomena, e.g. predicts the existence of the observed electrolytic domains, i.e. regions of negative current densities.

Keywords DMFC, membrane, characterization, methanol crossover, current distribution

ISBN (printed) 978-951-22-8980-6 | ISSN (printed) 1795-2239
ISBN (pdf) 978-951-22-8981-3 | ISSN (pdf) 1795-4584
ISBN (others) | Number of pages 90 p. + app. 56 p.

Publisher Department of Chemical Technology

Print distribution Laboratory of Physical Chemistry and Electrochemistry, P.O. Box 6100, 02015 TKK, Finland

☒ The dissertation can be read at http://lib.tkk.fi/Diss/2007/isbn9789512289813/

TEKNILLINEN KORKEAKOULU PL 1000, 02015 TKK http://www.tkk.fi	VÄITÖSKIRJAN TIIVISTELMÄ

Tekijä Ville Sakari Saarinen

Väitöskirjan nimi

TUTKIMUKSIA LIITTYEN SUORAMETANOLIPOLTTOKENNOON: PROTONIJOHTAVIEN POLYMEERIMEMBRAANIEN KARAKTERISOINTI JA KATODIN VIRRANJAKAUMAN TUTKIMINEN

Käsikirjoituksen jättämispäivämäärä 22.5.2007	Väitöstilaisuuden ajankohta 16.11.2007

☐ Monografia ☒ Yhdistelmäväitöskirja (yhteenveto + erillisartikkelit)

Osasto	Kemian tekniikka
Laboratorio	Fysikaalinen kemian ja sähkökemia
Tutkimusala	Polttokennot
Vastaväittäjä(t)	Professori Göran Lindbergh
Työn valvoja	Professori Kyösti Kontturi
(Työn ohjaaja)	TkT Tanja Kallio

Tiivistelmä

Väitöskirjassa on karakterisoitu uudenlaisia protonijohtavia suorametanolipolttokennomembraaneja käyttäen fyskaaliskemiallisia-, sähkökemiallisia- ja materiaalitieteen menetelmiä. Tutkimukset ovat pääasiassa keskittyneet tutkimaan sulfonoitua poly(etyleeni-*alt*-tetrafluoroetyleeni) (ETFE-SA) membraania, jota ei ole aiemmin tutkittu suorametanolipolttokennossa (DMFC). Muita tutkittuja membraaneja ovat sulfonoitu poly(phenyleeni sulfoni) (sPSO2), poly(vinylideenifluoridi)-*graft*-poly(styreeni sulfonihappo) (PVDF-*g*-PSSA) ja referenssimateriaalina kaupallinen Nafion® membraani. Membraanien turpoamisominaisuuksia on tutkittu erilaisissa alkoholi - vesi ja H_2SO_4 - vesi liuoksissa. Tutkimuksissa havaittiin vesi / alkoholi selektiivisyyden suhteen, että vettä suosiva selektiivisyys korreloi selvästi membraanin korkean ioninvaihtokapasiteetin (IEC) ja vähäisen turpoamisen kanssa. Lisäksi rikkihapon havaittiin vähentävän huomattavasti turpoamista, mikä merkitsee osmoosin olevan pääasiallisena ajavana voimana DMFC membraanien turpoamisprosessissa. Membraanien ominaisuuksia tutkittiin käyttäen erilaisia mikroskopiamenetelmiä (AFM, SEM & EDX, SECM) ja samalla demonstroitiin laajamittaisen karakterisoinnin etuja membraanien kehitystyössä. Membraanien pinnan hydrofobisuutta tutkittiin veden kontaktikulma (CA) menetelmällä. Eri membraanien pintaominaisuuksien havaitttiin poikkeavan selvästi toisistaan ja ETFE-SA membraanin suhteen tutkittiin myös valmistusparametrien vaikutusta membraanin ominaisuuksiin. Havaittiin, että ETFE-SA:lla on erittäin alhainen vedenottokyky, korkea vettä suosiva selektiivisyys eri alkoholien suhteen sekä hyvä kemiallinen ja mekaaninen stabiilisuus. Metanolin läpäisevyyttä membraanien läpi tutkittiin sekä diffuusiokennolla että todellisissa DMFC-olosuhteissa. Lisäksi membraaneja tutkittiin laboratoriomittakaavan DMFC-laitteistolla ja samalla selvitettiin yksityiskohtaisesti erilaisten käyttöparametrien välisiä riippuvuuksia. Yhtämittainen yli 2000 tunnin kestävyystesti DMFC:ssa ilman suorituskyvyn laskua vahvisti ETFE-SA:n käyttökelpoisuuden DMFC:ssa matalissa lämpötiloissa ($T < 80\ ^\circ C$). Metanolin läpäisevyyttä ja yleisemminkin aineensiirtoa tutkittiin myös erillisen vapaastihengittävän DMFC laitteiston avulla sekä myös käyttäen laskennallisia menetelmiä. Virranjakaumamittaukset tehtiin vastusverkon ja segmentodun katodin avulla. Kehitetty numeerinen 3D malli kuvaa laajasti vapaastihengittävän DMFC:n toimintaa ja aineensiirtoilmiöitä, esimerkiksi ennustaa mittattujen elektrolyyttisten alueiden (negatiivisten virrantiheyksien) esiintymistä.

Asiasanat DMFC, membraani, karakterisointi, metanolin läpäisy, virranjakauma

ISBN (painettu) 978-951-22-8980-6	ISSN (painettu) 1795-2239
ISBN (pdf) 978-951-22-8981-3	ISSN (pdf) 1795-4584
ISBN (muut)	Sivumäärä 90 s. + liit. 56 s.

Julkaisija Kemian tekniikan osasto

Painetun väitöskirjan jakelu Fysikaalisen kemian ja sähkökemian laboratorio, PL 6100, 02015 TKK

☒ Luettavissa verkossa osoitteessa http://lib.tkk.fi/Diss/2007/isbn9789512289813/

Preface

The work presented in this dissertation has been carried out in three years between 2004 and 2007 at the Laboratory of Physical Chemistry and Electrochemistry at Helsinki University of Technology (TKK) and at the Department of professor Joachim Maier at Max Planck Institute for Solid State Research, Stuttgart.

I would first like to acknowledge my supervisor, professor Kyösti Kontturi, for the guidance of my studies and for giving me the opportunity to do fuel cell research. I would like to thank my instructor Dr. Tanja Kallio for the advice and encouragement I got during the years. I would like to express my gratitude to emeritus professor Göran Sundholm for the support and interest in my research. Special thanks also to Dr. Klaus-Dieter Kreuer for welcoming me to Stuttgart and giving me the chance to work under his supervision. I thank Dr. Timo Laaksonen, Dr. Mikko Mikkola, Dr. Rotraut Merkle, Ms. Kirsi Yliniemi and Mr. Roope Telaranta for helping me in many practical things. Many thanks to all personnel of the Laboratory of Physical Chemistry and Electrochemistry for the very nice working atmosphere. Sincere thanks also goes to all the co-authors, especially to Mr. Olli Himanen, Mr. Mikko Karesoja and Dr. Mikael Paronen for the very fruitful collaboration.

I would like to thank my parents, Juhani and Marja-Leena, my sister Maippi and all other friends for the support and understanding you have given me during the years. Finally, many thanks to my wife, Patricia and my son, Saffert, whose smile always fills my life with joy and happiness.

Espoo, May 22nd, 2007

Ville Saarinen

Table of Contents

List of Publications

This thesis consists of an overview and of the following publications, which are referred to in the text by their Roman numerals.

I V. Saarinen, T. Kallio, M. Paronen, P. Tikkanen, E. Rauhala, K. Kontturi, *New ETFE-based membrane for direct methanol fuel cell*, Electrochim. Acta **50** (2005) 3453-3460.

II V. Saarinen, M. Karesoja, T. Kallio, M. Paronen, K. Kontturi, *Characterization of the novel ETFE-based membrane*, J. Membr. Sci. **280** (2006) 20-28.

III V. Saarinen, K.D. Kreuer, M. Schuster, R. Merkle, J. Maier, *On the swelling properties of proton conducting membranes for direct methanol fuel cells*, Solid State Ionics **178** (2007) 533-537.

IV V. Saarinen, O. Himanen, T. Kallio, G. Sundholm, K. Kontturi, *Current distribution measurements with a free-breathing direct methanol fuel cell using PVDF*-g-*PSSA and Nafion® 117 membranes*, J. Power Sources **163** (2007) 768-776.

V V. Saarinen, O. Himanen, T. Kallio, G. Sundholm, K. Kontturi, *A 3D model for the free-breathing direct methanol fuel cell: Methanol crossover aspects and validations with current distribution measurements*, J. Power Sources **172** (2007) 805-815.

Author's contribution

Publication I: All the measurements were done by the author, who was also responsible for the data analysis and acted as the main author of the publication.

Publication II: The author performed or participated in all of the measurements and did the data analysis. The author acted as the main author of the publication.

Publication III: The author made all the measurements and the data analysis. He wrote the first version of the publication and was actively involved in the writing process and interpretation of the results.

Publication IV: The author designed the measurements and performed or participated in all of the experimental work. The data analysis was made by the author and he acted as the main author of the publication.

Publication V: The author participated actively in the modelling work and the implementation of the model. The author acted as the main author of the publication.

The ETFE-SA membranes investigated in this thesis were made by Dr. Mikael Paronen, the PVDF-*g*-PSSA membranes by Dr. Nadia Walsby and the sPSO2 membranes by Dr. Michael Schuster.

Espoo, May 22nd, 2007

Professor Kyösti Kontturi

List of Abbreviations

Aciplex®	Sulphonated tetrafluorethylene copolymer (Asahi Chemicals)
AFC	Alkaline fuel cell
AFM	Atomic force microscopy
CA	Contact angle
DMA	Dynamic mechanical analysis
DMFC	Direct methanol fuel cell
d.o.g.	Degree of grafting
d.o.s.	Degree of sulphonation
Dow®	Sulphonated tetrafluorethylene copolymer (Dow Chemical)
DSC	Differential scanning calorimetry
ETFE-SA	Sulphonated poly(ethylene-*alt*-tetrafluoroethylene)
EW	Equivalent weight
EDX	Energy dispersive X-ray analysis
EtOH	Ethanol
FEP	Poly(tetrafluoroethylene-*co*-hexafluoropropylene)
Flemion®	Sulphonated tetrafluorethylene copolymer (Asahi Glass)
FP	Fluoropolymer
GDL	Gas diffusion layer
HFP	Hexafluoropropylene
IEC	Ion exchange capacity
LU	Liquid uptake
M	Monomer
MCFC	Molten carbonate fuel cell
MEA	Membrane electrode assembly
MeOH	Methanol
MS	Mass spectrometry
Nafion®	Sulphonated tetrafluorethylene copolymer (Du Pont)
OCV	Open circuit voltage

ORR	Oxygen reduction reaction
PAFC	Phosphoric acid fuel cell
PEEK	Poly(etheretherketone)
PEFC	Polymer electrolyte fuel cell
PEM	Proton exchange membrane
PS	Polysulphone
PSSA	Polystyrene sulphonic acid
PTL	Porous transport layer
PTFE	Poly(tetrafluoroethylene)
PVDF-*g*-PSSA	Poly(vinylidenefluoride)-*graft*-poly(styrene sulphonic acid)
2-PrOH	2-Propanol
RH	Relative humidity
SA	Sulphonic acid
SECM	Scanning electrochemical microscopy
SEM	Scanning electron microscopy
SOFC	Solid oxide fuel cell
sPSO2	Sulphonated poly(phenylene sulphone)
*t*BuOH	*Tert*-Butanol
TEM	Transmission electron microscopy
TFE	Tetrafluorethylene
TGA	Thermogravimetric analysis
TG	Thermogravimetry
WAXS	Wide angle X-ray scattering
WU	Water uptake

List of Symbols

A	Area (m^2)
c	Concentration (mol m^{-3} or M)
D	Diffusion coefficient (m^2 s^{-1})
E	Potential (V)
E^0	Standard potential (V)
E'	Storage modulus (Pa)
E''	Loss modulus (Pa)
F	Faraday's constant (96 485 C mol^{-1})
G	Gibbs free energy (J mol^{-1})
$\mathbf{g}$	Acceleration due to gravity (9.81 m s^{-2})
H	Enthalpy (J mol^{-1}) or Partition coefficient
I	Current (A)
i	Current density (A m^{-2})
i_0	Exchange current density (A m^{-2})
i_{lim}	Limiting current density (A m^{-2})
$[i_{\text{t}}\sqrt{t}]^2_{\text{Cot}}$	Cottrell slope (A^2 m^{-4} s)
k_{dl}	Electro-osmotic drag correction coefficient for Cottrell slope
k_{dt}	Electro-osmotic drag correction coefficient for i_{lim}
l	Thickness (m)
M	Molar mass (kg mol^{-1})
m	Mass (kg)
$\mathbf{N}$	Molar flux (mol m^{-2} s^{-1})
n	Number of electrons or Amount of substance (mol)
N_{A}	Avogadro's constant (6.022×10^{23} mol^{-1})
P	Permeability (m s^{-1})
p	Pressure (Pa or atm)
R	Universal gas constant (8.314 J mol^{-1} K^{-1}) or Resistance (Ω)
R_{A}	Area resistance (Ω m^2)

S	Selectivity
$tan\,\delta$	Loss tangent
T	Temperature (K or °C)
T_g	Glass transition temperature (K or °C)
t	Time (s)
$\mathbf{u}$	Velocity (m s^{-1})
V	Voltage (V) or Volume (m^3)
$\dot{V}$	Flow rate (m^3 s^{-1})
X	Mole fraction
x	Moisture ratio
z	Electric charge

Greek

α	Transfer coefficient of electrochemical reaction
Δ	Difference
ϵ	Porosity
η	Efficiency or Overpotential (V)
κ	Intrinsic permeability (m^2)
λ	Solvent content or Stoichiometry or Electro-osmotic drag coefficient
μ	Dynamic viscosity (kg m^{-1} s^{-1})
ρ	Density (kg m^{-3})
σ	Conductivity (S m^{-1})
Σv	Diffusion volume
ϕ	Potential (V)
ψ	Parameter for MeOH oxidation rate at cathode (m s^{-1})

Subscripts and superscripts

0	Reference or Initial value
a	Anode
act	Activation

amb	Ambient
ave	Average
B	Bulk
cell	Fuel cell
c	Cathode
conc	Concentration
cr	Critical
eff	Effective
ele	Electrode
g	Gaseous
gdl	Gas diffusion layer
graf	Grafted
i	Species
j	Species
liq	Liquid
lim	Limiting
m	Protonic phase
mem	Membrane
ohm	Ohmic
ptl	Porous transport layer
ref	Reference
s	Surface or Electronic phase
sol	Solution

1 Introduction

1.1 Background

Fuel cells are conversion devices, which convert the chemical energy released in electrochemical reactions directly into electrical energy. The fuel used is typically a hydrocarbon or a substance derived from it or based on it, e.g. hydrogen or alcohol. The first operating fuel cell has already been built in 1839 by Sir William R. Grove [1] and after that several types of fuel cells have been developed. The fuel cells are normally classified according to the type of electrolyte and operation temperature: The low temperature fuel cells are AFC (Alkaline Fuel cell), PAFC (Phosphoric acid fuel cell), PEFC (Polymer electrolyte fuel cell) and DMFC (Direct methanol fuel cell). The DMFC differs from PEFC by the anode reactant, which is a liquid mixture of water and methanol (MeOH) instead of gaseous hydrogen in the PEFC. The high temperature fuel cells are SOFC (Solid oxide fuel cell) and MCFC (Molten carbonate fuel cell). This thesis concerns only the DMFC and more detailed descriptions of other fuel cell types can be found in literature [1–3].

The PEFC was invented by William T. Grubb, who first suggested the use of cation exchange membrane as an electrolyte in the fuel cell in 1955 [4–6]. The very first fuel cell system based on a sulphonated polystyrene electrolyte was then developed in the 1960s as an on-board power source in the Gemini space program [2]. This PEFC system was developed using a great amount of noble metal at the electrodes, although the polystyrene sulphonate hydrocarbon membrane was not electrochemically stable and the cell exhibited limited power density (less than 50 mW cm^2) [7]. The life-limiting factor in these membranes was the oxidative degradation of the C–H bonds and later on the development of PEFCs had been strongly related to the improvements of the polymer electrolyte membrane [8]. Two major improvements were made in the PEFC technology after the Gemini program: The first was the development of the more stable perfluorosulphonic acid membranes, i.e. Nafion®

membranes, started in 1962 by E. I. du Pont de Nemours and Company [9]. The second big development step took place in 1965, when Niedrach *et al.* invented thin film electrodes for the PEFC, which enabled greater catalyst surface area and thus, the required amount of expensive platinum catalyst could be significantly decreased [10, 11]. During recent years, thin-film electrodes were developed further on [12–14] and also different kinds of manufacturing techniques of electrodes were introduced [15, 16].

During the last two decades several companies around the world have been focused on the commercialization of the fuel cells for stationary power, and at the moment almost all of the major automotive companies have either internal fuel cell development programs or they are working closely with other companies to develop power plants for transportation applications [8]. Also, some PEFC and DMFC demonstrations and prototypes have been developed for electric vehicles [17, 18], military applications [19, 20], aircrafts [21, 22] and submarines [23]. In the case of the small scale power production, a general trend nowadays is that the size of all portable electronic devices decrease, but the power consumption increases at the same time. Practically, it means that conventional primary and rechargeable batteries are soon becoming inadequate for the increasing power requirements of portable electronic devices [24].

Already today the limitations of battery capacity cause e.g. the main restrictions of the wireless use of laptop computers. The alternative power supply in the future could be the DMFC [25]. However, the best power densities achieved at the moment are still too low for commercial applications or the price is too high. Thus, in order to make the DMFCs competitive against other energy production methods, they should achieve much higher power densities and at the same time, lower manufacturing and operating costs. It has been assumed that the DMFC power densities of 300 W dm^{-3} and 1 kW dm^{-3} can be achievable under conditions applicable to portable power and transport applications, respectively [26]. The PEFCs can also

be used for portable power production [27, 28], but the use of MeOH gives some advantages compared to the hydrogen systems: the storage of fuel is easier and the systems can have a simpler structure. Methanol has a higher energy density than hydrogen - according to Ref. [29]: MeOH: 17×10^9 J m^{-3} (100 wt-%, 25 °C), H_2: 0.6×10^9 J m^{-3} (6.9×10^6 Pa, 25 °C). Also, the storage of MeOH is easier, because MeOH is liquid at room temperature, whereas hydrogen is a gas.

Overall, there are many challenges in designing small scale DMFC systems, but it is especially desirable that the system is simple. An attractive way for simplification of the DMFC system is to use natural air convection at the cathode and no MeOH pumps. As a comparison, there can be some difficulties in the storing of hydrogen in very small packages and the integration of the auxiliary devices needed for hydrogen handling can be problematic. Therefore, the DMFCs are a very promising alternative for small scale energy production, especially for portable electronic devices. In this field, there are already some semi-commercial products available now or in the near future, e.g. a 20 W portable DMFC system having higher energy density than lithium batteries [30], a micro DMFC system for IBM ThinkPad notebook computers [31] and a DMFC powered 300 mW mobile audio player and cell phone from Toshiba and Hitachi [32].

1.2 Motivation and Objectives

Fuel cells offer many favourable characteristics compared to the conventional energy conversion devices. One of the major factors that have influenced the development of fuel cells is the environmental point of view: Reduction of pollution has become a matter of great concern and there is a true need for cleaner and more efficient energy conversion methods. Fuel cells are an environmentally friendly way to produce electricity and they can help us to reduce our dependence on fossil fuels and consequently to reduce harmful emissions into the atmosphere. Fuel cells can be operated flexibly using many commonly available fuels such as natural gas, other

hydrocarbons, hydrogen or alcohols.

When pure hydrogen is used directly as a fuel, only water is generated and no pollutants are emitted. The DMFC also produces carbon dioxide, but the amounts of CO_2 are significantly lower compared to e.g. combustion engines, due to higher overall efficiency. The fuel cell efficiency is not limited by the Carnot cycle and fuel cells are potentially far more efficient than the classical combustion engines. In addition, the efficiency of the fuel cell is also almost independent of the electric load. This makes fuel cells very suitable for applications such as vehicles, where good efficiency is desired also far from the peak power. Because of exothermic chemical and electrochemical reactions, fuel cells have also a capability of co-generation of electricity and heat. Fuel cell systems can also be scaled easily up and down, ranging from a few watts to megawatts. Thus, the fuel cells are expected to serve on one hand as large power plants, and on the other hand as a power source for portable electronic devices. The absence of moving parts improves reliability and reduces maintenance costs by reducing maintenance requirements. Because of the reason mentioned earlier, the operation of fuel cells is quiet and there is no noise pollution.

At the moment, the main obstacle of the DMFC commercialization is the cost of the technology. Even though most of the needed technology is already available, there are many open questions on a way towards the large-scale use of the fuel cells such as the choice of the fuel and its storage, the treatment of the produced heat and the optimization of both the infrastructure and transportation of the reactants. A lot of challenges also exist concerning both the optimization of materials and structure of the fuel cell components (membrane, electrodes, porous transport layers and bipolar plates) and whole fuel cell stack and auxiliary equipment. In order to take the remaining steps towards the real DMFC applications, a lot of DMFC development work has to be done: all promising candidates as new DMFC materials are needed to be examined and both their properties and compatibility with the DMFC system needs to be comprehensively clarified.

As a part of this bigger frame, this thesis is focused on investigations of novel DMFC membranes. An important goal in the DMFC research is to develop cheaper electrolytes that would operate at least as well as the membranes based on poly(perfluorosulphonic acid), e.g. the commercial Nafion® membranes. The drawback of these nowadays widely used Nafion® membranes is especially their high methanol permeability (MeOH crossover) [33, 34]. In consequence, only dilute MeOH mixtures (0.5 - 2 M) can be used to achieve optimum power production. Thus, the development of more MeOH impermeable membranes can be considered as one of the main issues of the DMFC research at the moment.

In this thesis, new membranes are characterized widely by combining methods of physical chemistry, electrochemistry and material science. Different kinds of membranes are characterized extensively with sophisticated methods and their properties are compared to the commercial Nafion® membranes. This work is mainly focused on sulphonated poly(ethylene-*alt*-tetrafluoroethylene) (ETFE-SA) membrane, which has not been used in a DMFC prior to these studies. The ETFE-SA membrane has some very attractive properties from the view point of DMFC applications and its price is substantially lower compared to the Nafion® membranes.

The other main topic in this study is to investigate mass transfer phenomena both in the membrane and in the whole DMFC system with a free-breathing DMFC using natural convection as the air supply method. The investigations are concentrating mainly on the MeOH crossover phenomenon, which is one of the biggest concerns in the DMFC systems at the moment. There are also numerous other interrelated parameters in the DMFC system and the connections between different operation parameters can be clarified experimentally. This information is valuable from the view point of the membrane and electrode development and for the fuel cell modelling.

1.3 Outline of This Thesis

The thesis starts with a brief introduction to fuel cells and continues with a detailed description of the direct methanol fuel cell (DMFC). In Chapter 2, the structure and operational principle of the DMFC are explained and in Chapter 3 electrode reactions, different loss mechanisms and aspects concerning efficiency and both the ideal and the real performance of the DMFC are discussed.

In the beginning of Chapter 4, different types of proton conducting membranes are described and an overview concerning their properties and challenges are given. All the investigated membranes are presented and their main properties are described at the end of Chapter 4. The experimental and computational methods used in this thesis are presented in Chapter 5 including surface and structural analysis, swelling and permeability, DMFC testing, current distribution measurement and DMFC modelling sections.

The results achieved in this thesis are summarized in Chapter 6 and especially the properties of the investigated membranes are compared and implications of their use in the DMFCs are discussed. The benefits of the extensive membrane characterization and its connections to the membrane development work are demonstrated. Also, the results gained with the experimental current distribution measurement system are presented and the features of the 3D model developed for the free-breathing DMFC are discussed. A summary and concluding remarks are given in Chapter 7.

2 Direct Methanol Fuel Cell

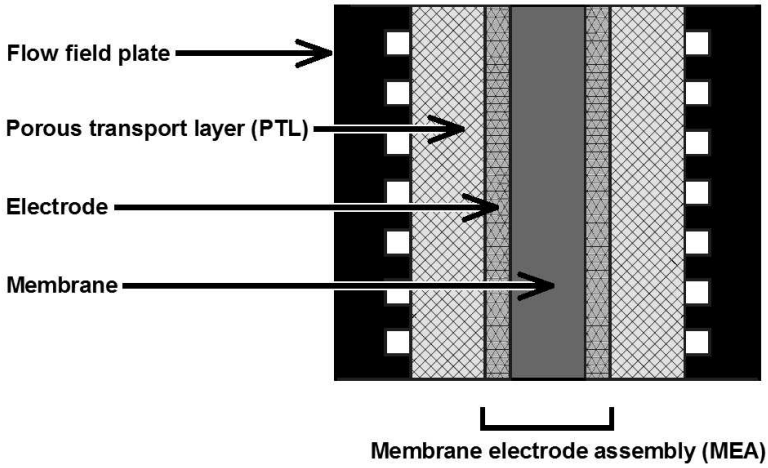

Figure 2.1: The schematic structure and the main components of the DMFC.

2.1 Structure and Operational Principle

The direct methanol fuel cell (DMFC) is a polymer electrolyte fuel cell (PEFC), where the anode reactant is an aqueous mixture of methanol. The main parts of the DMFC are the proton conducting membrane, the electrodes, the porous transport layers (PTLs) and the flow field plates. The schematic structure and main components of the DMFC are presented in Fig. 2.1. The electrochemical reactions occur at the electrodes: MeOH molecules are oxidized at the anode and the reduction reaction of oxygen takes place at the cathode. The electrodes are separated by the proton conducting polymer membrane, in which the negative ions are immobilized in a polymer matrix. The protons and electrons generated at the anode are consumed in the cathode reactions, where they react with O_2 molecules. As a result from the interphase potentials at the electrodes, a potential difference is formed between them and the DMFC can be used as a source of electrical current by connecting the electrodes to an external load. The overall DMFC reaction is an

exothermic reaction, i.e. the cell also produces heat. Other main reaction products are water at the cathode and carbon dioxide at the anode. A detailed description of the electrochemical reactions occurring in the DMFC is presented in Chapter 3.

2.2 Proton Conducting Membrane

In the center of the DMFC is a proton conducting membrane. The solid polymer electrolyte provides ionic conductivity, prevents the flow of electrons, acts as a barrier to the reactants and maintains chemical and mechanical stabilities [7]. The typical thickness of the PEFC and the DMFC membranes is in the range of 30-200 μm and many different kinds of membranes have been developed during the years, see e.g. review articles of Souzy *et al.* [7], Mehta *et al.* [15], Kreuer *et al.* [35], Gubler *et al.* [36], Deluca *et al.* [37], Hickner *et al.* [38] and Neburchilov *et al.* [39]. The membranes of the DMFC can be quite similar to the ones used in the PEFC, but they should additionally have a low permeability for MeOH in order to avoid efficiency losses due to the MeOH crossover phenomenon. Therefore, the DMFC membranes are normally somewhat thicker than the PEFC membranes.

Most of the investigated polymer membranes are partially or fully fluorinated and there exist various synthesization routes for them. Those synthesization methods can be separated into three main families of alternatives [7]: The first concerns direct radical copolymerization of fluoroalkenes with fluorinated functional monomers, which are either fluorinated vinyl ethers, α,β,β-trifluorostyrenes or trifluorovinyl oxyaromatic monomers bearing sulphonic or phosphonic acids. The best known example of this first group of membranes is the Nafion® membrane. The second route deals with the chemical modification of hydrogenated polymers (e.g. polyparaphenylenes) with fluorinated sulphonic acid synthons [7]. The third alternative concerns the synthesis of FP-*g*-poly(M) graft copolymers where FP and M stand for fluoropolymer and monomer, respectively, obtained by activation (e.g. irradiation arising from electrons, protons or γ-rays or chemical activation with ozone) of

FP polymers followed by grafting of M monomers. The most used M monomer is styrene, and a further step of sulphonation on FP-g-PS leads to FP-g-PS sulphonic acid graft copolymers. The PVDF-g-PSSA membrane investigated in this thesis is a typical example of this third group of membranes, whereas the ETFE-SA membrane is a membrane functionalized by irradiation and direct sulphonation.

In many cases non-fluorinated membranes have a poor resistance against oxidation and thermal degradation, but some non-fluorinated membranes have also been developed, e.g. sulphonated polystyrenes, sulphonated polyimides, sulphonated poly(aryl ether sulphone)s, sulphonated poly (aryl ether ketone)s, sulphonated phenol formol resins, sulphonated poly(phenylene oxide)s, sulphonated poly(p-phenoxybenzoyl-1,4-phenylene)s, phosphonic poly(phenylene oxide)s, sulphonated silicates, sulphonated poly(benzimidazole)s, sulphonated organic-inorganic hybrids and polyphosphazenes [7, 15, 38, 40–42]. The only non-fluorinated membrane included in this thesis is the sPSO2 membrane. In addition to the above mentioned membranes, also a wide range of different kinds of composite membranes or surface modified membranes have been developed [7]. One well-known example is the ultra-thin composite membrane made by reinforcing a perfluorosulphonic acid membrane with a porous PTFE sheet introduced by W. L. Gore [43, 44].

2.3 Electrodes

The DMFC electrodes typically contain expensive noble metal catalysts, which are used in order to achieve a sufficient reaction rate at low temperatures. The electrochemical oxidation of MeOH is more complicated than the oxidation of hydrogen, resulting in higher activation overpotentials. Because of the higher activation overpotentials and the MeOH crossover phenomenon, the power densities gained from the DMFCs are substantially lower compared to the PEFCs. Normally platinum is used at the cathode and alloyed platinum-ruthenium (1:1) at the anode of the DMFC. Ruthenium is used to enhance the tolerance of the catalyst against CO

poisoning. Other alternatives for catalyst materials have also been investigated, e.g. Pt_3Sn/Pt-Ru [45], Pt_3Sn/Pt-Pd [46], Pt-Ru-Sn/Pt-Ru [47] and Pt/Mo [48], but none of them have been proven to be more suitable for the DMFC than the Pt/Pt-Ru catalyst.

In order to obtain useful current densities from the DMFC, the electrode needs to have high surface area compared to the geometric area. The catalyst particles of the electrodes must be located so that they can form a three-phase boundary, i.e. they are in contact with both the electronic and protonic phase and there are free routes for the reactants to reach the catalyst sites. In addition, the proton conducting phase in the electrode region must be hydrated in order to be proton conductive. Thus, the efficiency of the catalyst reactions can be improved substantially by enhancing the active surface area of the catalyst and ensuring uniform distribution of the catalyst particles [49]. Because of the high price of the noble metals, it is important to have a low catalyst loading in the electrodes. As a solution, the thin-film electrodes have been developed [12–14]. The thin-film electrodes consist of a porous layer of proton conducting phase and high surface area carbon black particles coated with smaller size catalyst particles [13, 14, 50]. The typical thickness of the thin-film electrode used in the DMFC is some micrometers and the Pt/Pt-Ru loading is typically in the range of 0.5-5 mg cm^{-2}. Also, a wide range of other catalyst materials and manufacturing techniques of electrodes for the PEFC and the DMFC have been investigated during the years, see e.g. Refs [15, 16, 51–55]. In practice, the efficiency of the electrodes can also be increased by adjusting the operational parameters, e.g. by setting both the optimal MeOH concentration for the anode and the optimal back-pressure of oxygen for the cathode [56].

2.4 MEA and Porous Transport Layers

The membrane and electrodes together are usually called a membrane electrode assembly (MEA), which is sandwiched between the porous transport layers (PTLs)

in the DMFC. The commonly used manufacturing technique of the MEA is hot-pressing, where electrodes are compressed together with a membrane at elevated temperatures (120-160 °C). Prior to hot-pressing the electrodes (catalyst particles) are sprayed, sputtered or electrodeposited on the surface of the membrane or the PTL.

A reasonable mechanical strength and moderate dimensional changes are required for the membranes and the electrodes during the manufacturing process of the MEA and also during the incorporating of the MEA into the DMFC system and the fuel cell operation. [7]. In the case of the PEFC and with only gaseous reactants, the PTLs are conventionally called also gas diffusion layers (GDLs). The purpose of the PTLs is to form an electronic and thermal contact between the electrodes and the flow field plates and to provide transport paths for the reactants. Thus, the PTLs should have a high electrical and thermal conductivity, good chemical and mechanical properties and high porosity [57–59].

The typical PTL materials are carbon-based papers, felts or cloths and they normally have a macroporous backing layer and a microporous diffusion layer applied on one or both sides of the backing layer [60–63]. In some studies [64] also metallic materials have been used as a PTLs, but their properties are usually unfavourable compared to carbon based materials. The typical thickness of the PTL is in the range of 300-400 μm and there are also commercial gas diffusion electrodes, where electrodes are combined to the PTLs during the manufacturing. For further information on the PTL materials and their characterization, see e.g. the review article of Mathias *et al.* [65].

2.5 Flow Field Plates and Auxiliary Equipment

The MEA and PTLs are located between the flow field plates i.e. bipolar plates or end plates, which normally have channels on the surfaces facing the PTLs. The

channels provide a route for the distribution of the reactants to the electrodes and the removal of reaction products. The flow field plates also provide mechanical support for the DMFC and electrical connection between the unit cells in the fuel cell stack. The materials of the flow field plates should have a high electrical and thermal conductivity, good mechanical properties and high chemical stability. The most commonly used material for the flow field plates is a resin impregnated graphite. Because graphite is quite expensive and difficult to machine also other materials have been investigated, e.g. metallic materials with corrosion-resistant surface treatment [66–71] or composite materials of carbon and polymers [72–74].

Because a single DMFC cell delivers voltage less than 1 V, the unit cells are connected in series to a DMFC stack to obtain higher voltages. The fuel cell stack geometry, as well as the channel geometry of the flow field plates of the unit cells, affects significantly the efficiency of mass transport in the cell. As practical solutions, different types of cell geometries have been introduced, e.g. planar cells [75], annular cells [76, 77] and in a very small scale even miniaturized fuel cells on silicon wafer [78, 79]. Typically in the fuel cells oxygen or air is fed by forced convection into the cathode in order to decrease mass transfer losses. However, especially for the small DMFC systems all auxiliary equipment such as MeOH pumps, oxygen or air bottles, mass flow and temperature controllers and heating elements decrease notably the volumetric energy density. Thus, it would be advantageous to use free-breathing DMFC systems in e.g. portable electronic devices, even though the free convection of air increases oxygen mass transfer losses due to unregulated oxygen stoichiometry.

3 Electrochemical Reactions and Cell Potentials

3.1 Galvanic and Electrolytic Domains

According to experimental results in Publication IV and observations of e.g. Ye *et al.* [80] and Kulikovsky *et al.* [81], two different regions can be distinguished inside the DMFC depending on the local conditions:

1. Normal DMFC operation (Galvanic cell):

$$\text{Anode:} \qquad CH_3OH + H_2O \longrightarrow CO_2\ (g) + 6H^+ + 6e^- \tag{3.1}$$

$$\text{Cathode:} \qquad \frac{3}{2}O_2\ (g) + 6H^+ + 6e^- \longrightarrow 3H_2O \tag{3.2}$$

$$\text{Overall reaction:} \qquad CH_3OH + \frac{3}{2}O_2 \longrightarrow CO_2\ (g) + 2H_2O \tag{3.3}$$

2. Electrolytic cell:

$$\text{Anode:} \qquad 6H^+ + 6e^- \longrightarrow 3H_2\ (g) \tag{3.4}$$

$$\text{Cathode:} \qquad CH_3OH + H_2O \longrightarrow CO_2\ (g) + 6H^+ + 6e^- \tag{3.5}$$

$$\text{Overall reaction:} \qquad CH_3OH + H_2O \longrightarrow CO_2\ (g) + 3H_2\ (g) \tag{3.6}$$

Reaction 3.2 is the main reaction at the cathode of the DMFC, but because of the MeOH crossover phenomenon, MeOH oxidation will also occur at the cathode according to Reaction 3.5. The MeOH permeating from the anode to the cathode poisons the Pt catalyst and causes mixed potentials, which decrease the fuel cell performance [82, 83]. The polarization losses result mainly from the heterogeneous oxidation of MeOH in the presence of oxygen [84]. Ye *et al.* [85] have observed a significant decline of the open circuit voltage (OCV) in the DMFC, when the oxygen flow rate is reduced below a critical value. This can be explained by the

coexistence of galvanic and electrolytic reactions in the DMFC, even when the cell is operated under open circuit conditions [80, 81]. These reactions produce self-discharging currents in the DMFC causing MeOH consumption and H_2 evolution (Reaction 3.4). On the contrary, when the oxygen flow rate is above the critical value, the OCV is observed to be very insensitive to this quantity [85]. When the MeOH crossover rate through the membrane is low, Reaction 3.2 is dominating at the cathode. The MeOH crossover through the membrane is caused by water / MeOH transport and its coupling to the transport of protonic charge carriers [86,87]: water / MeOH diffusion and permeation are prevailing at low current densities, electro-osmotic protonic drag is controlling crossover at high current densities. The electro-osmotic drag in polymer membranes have also been investigated in many studies [88–93].

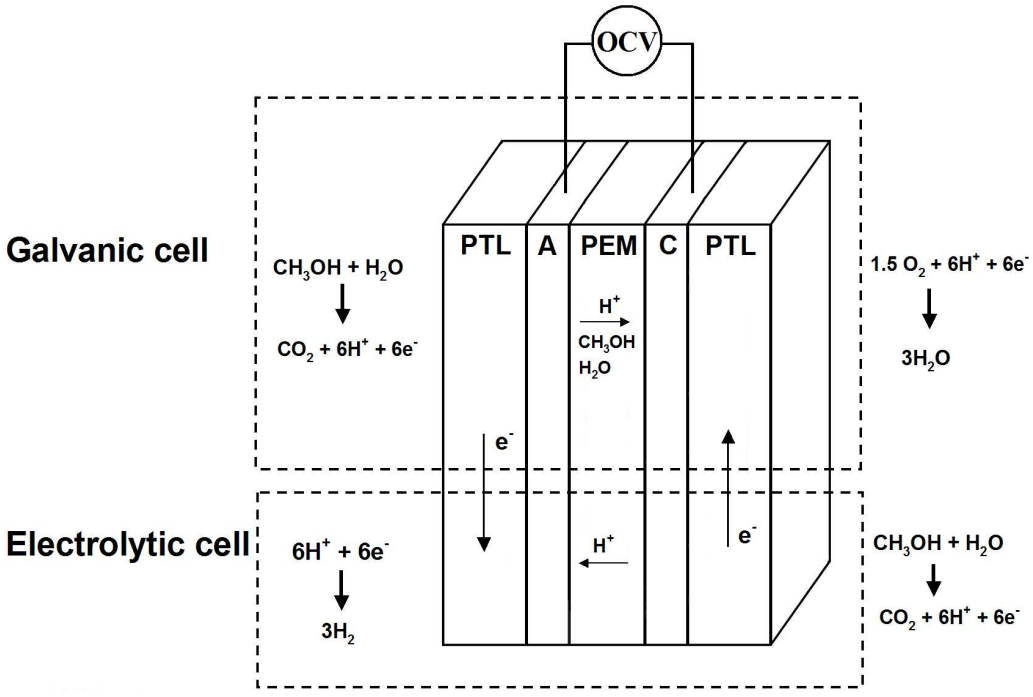

Figure 3.1: The electrochemical reactions in galvanic and electrolytic regions of the DMFC.

3.2 Electrode Kinetics

The reaction kinetics in the DMFC are more complicated than in the H_2-fed PEFC, because in addition to the actual DMFC reactions (Eqs. 3.1 - 3.3), many side reactions can take place. Because of simplicity, the electrode kinetics and all possible DMFC reactions are presented here only for the normal DMFC operation (Galvanic cell) neglecting transport of all species through the membrane. The electrode kinetics at the DMFC anode are by nature very slow and only platinum and Pt-based electrode materials are capable of adsorbing MeOH in acid solution. Only on these materials the reaction rate for MeOH oxidation becomes high enough for practical applications. On platinum, the catalytic reaction of MeOH is believed to take place in several steps [16, 94]. First the MeOH molecule is dissociatively adsorbed on the Pt-catalyst and the protons are detached one by one:

$$CH_3OH + Pt\ (s) \longrightarrow Pt - CH_2OH^{\bullet} + H^+ + e^- \tag{3.7}$$

$$Pt - CH_2OH^{\bullet} + Pt\ (s) \longrightarrow Pt_2 - CHOH^{\bullet} + H^+ + e^- \tag{3.8}$$

$$Pt_2 - CHOH^{\bullet} + Pt\ (s) \longrightarrow Pt_3 - COH^{\bullet} + H^+ + e^- \tag{3.9}$$

$$Pt_3 - COH \longrightarrow Pt - CO + 2Pt\ (s) + H^+ + e^- \tag{3.10}$$

As a result of Reaction 3.10, linearly bound carbon monoxide molecule is formed. This effectively poisons the catalyst until the potential becomes high enough for the water molecule to react with a Pt-atom to form an adsorbed hydroxyl group [16]:

$$Pt\ (s) + H_2O \longrightarrow Pt - OH + H^+ + e^- \tag{3.11}$$

The next reaction step is either (3.12) or (3.13) and finally Reaction (3.14) takes place and gaseous carbon dioxide is formed [16]:

$$Pt - OH + Pt - CO \longrightarrow Pt - COOH^{\bullet} \tag{3.12}$$

$$Pt - CO + H_2O \longrightarrow Pt - COOH^{\bullet} + H^+ + e^- \tag{3.13}$$

$$Pt - COOH^{\bullet} \longrightarrow Pt\ (s) + CO_2\ (g) + H^+ + e^- \tag{3.14}$$

Other suggested [16] side reactions, which can take place at the DMFC anode are Reactions (3.15)-(3.19):

$$Pt - CH_2OH \longrightarrow Pt\ (s) + HCHO^{\bullet} + H^+ + e^- \tag{3.15}$$

$$Pt_2 - CHOH^{\bullet} + Pt - OH^{\bullet} \longrightarrow 3Pt\ (s) + HCOOH + H^+ + e^- \tag{3.16}$$

$$Pt_2 - CHOH^{\bullet} + H_2O \longrightarrow 2Pt\ (s) + HCOOH + 2H^+ + 2e^- \tag{3.17}$$

$$Pt_3 - COH^{\bullet} + Pt - OH^{\bullet} \longrightarrow 3Pt\ (s) + Pt - COOH + H^+ + e^- \tag{3.18}$$

$$Pt_3 - COH^{\bullet} + H_2O \longrightarrow 2Pt\ (s) + Pt - COOH^{\bullet} + 2H^+ + 2e^- \tag{3.19}$$

The active site, where a new MeOH molecule could adsorb is not free until Reaction (3.14) has taken place. The activity of the Pt-catalyst can be increased by alloying it with another metal, which becomes oxidized easier than platinum. Hogarth *et al.* [95] have proved that Pt-Ru alloys have much higher activity than pure platinum. The water molecule can adsorb on ruthenium at lower potentials compared to platinum and form Ru-OH. At the same time adsorbed CO on platinum can react with Ru-OH and form CO_2. As a result, the hydroxyl groups on ruthenium enhance significantly CO removal and CO_2 formation at the DMFC anode [95].

The platinum catalyst enhances also significantly the oxygen reduction reaction (ORR) at the DMFC cathode. Because of the MeOH crossover phenomenon, the MeOH oxidation will also occur at the cathode causing shortage of active sites for oxygen molecules. The cathode Pt catalyst is more vulnerable to CO poisoning than the anode Pt-Ru due to adsorbed hydroxyl groups on ruthenium. The CO poisoned platinum will remain covered with CO at the cathode, unless the temperature or potential is risen to induce the thermal desorption or oxidation of CO molecules [82, 83]. Even though the MeOH crossover and mass transport of species through the membrane are neglected, the following five reduction reactions and one oxidation reaction can exist at the DMFC cathode [16]:

$$O_2\ (g) + 4H^+ + 4e^- \longrightarrow 2H_2O \qquad \text{[E=1.23 V]} \tag{3.20}$$

$$PtO_2 + 2H^+ + 2e^- \longrightarrow Pt(OH)_2 \qquad \text{[E=1.1 V]} \tag{3.21}$$

$$Pt(OH)_2 + 2H^+ + 2e^- \longrightarrow Pt + 2H_2O \qquad \text{[E=0.98 V]} \tag{3.22}$$

$$PtO + 2H^+ + 2e^- \longrightarrow Pt + H_2O \qquad \text{[E=0.88 V]} \tag{3.23}$$

$$O_2 + 2H^+ + 2e^- \longrightarrow H_2O_2 \qquad \text{[E=0.68 V]} \tag{3.24}$$

$$HO_2 \longrightarrow O_2\ (g) + H^+ + e^- \qquad \text{[E=0.13 V]} \tag{3.25}$$

3.3 Efficiency and Theoretical Cell Potentials

The theoretical efficiency η of the DMFC is determined as the change in *Gibbs free energy* divided by the change in enthalpy:

$$\eta = \frac{\Delta G^\circ}{\Delta H^\circ} \times 100\% \tag{3.26}$$

For the DMFC overall reaction (Eq. 3.3) in standard conditions (298.15K, 1 atm) ΔG$^\circ$ = -702 kJ mol^{-1} and ΔH$^\circ$ = -727 kJ mol^{-1}. Thus, the theoretical efficiency η for the DMFC is as high as 97%. As a comparison, the theoretical maximum efficiency for a Carnot cycle limited combustion engine (burning temperature of fuel 2600 K and exiting gas temperature 1000 K) is about 60% and because of losses, in practise only values of 10-30% can be achieved for conventional engines. The efficiency of the fuel cell is not significantly affected by the size of the cell, whereas in heat engines or combustion engines the efficiency typically decreases with decreasing size. The theoretical open circuit potential E$^\circ$ for the DMFC can be calculated according to the definition of the change in Gibbs free energy:

$$E^\circ = -\frac{\Delta G^\circ}{nF} \tag{3.27}$$

where n is the number of electrons ($n = 6$) transferred in the cell reaction. For the DMFC the theoretical open circuit potential E$^\circ$ is 1.21 V. In general, any cell reaction for the DMFC can be written as:

$$aA + bB \longrightarrow cC + bB \tag{3.28}$$

The effect of activity (concentration) of reactants on the cell potential E can be then calculated according to the *Nernst equation* [2]:

$$E = E^{\circ} + \frac{RT}{nF} ln \frac{[A]^a [B]^b}{[C]^c [D]^d} \tag{3.29}$$

3.4 Overpotentials and Polarization Curve

The real electrode reactions differ from the theoretical and that decreases total cell performance and efficiency. The actual DMFC open circuit voltage (OCV) is less than the ideal cell voltage predicted by the *Nernst equation* (Eq. 3.29), because of different loss mechanisms, i.e. overpotentials. The total overpotential η is the sum of activation overpotential η_{act}, resistive losses (iR drop) and concentration overpotential η_{conc}.

$$\eta = |\eta_{\text{act}}| + |iR| + |\eta_{\text{conc}}| \tag{3.30}$$

At low current densities, the DMFC performance is mostly limited by the electron transfer and this loss mechanism is called activation overpotential η_{act}. At medium current densities, the resistive losses of the DMFC system, i.e. ohmic overpotential η_{ohm}, become significant and can be described with *Ohm's law*:

$$\eta_{\text{ohm}} = iR \tag{3.31}$$

where the total cell resistance R is the sum of electronic, ionic and contact resistances. At high current densities, the electrode reactions proceed much faster than mass transport of the reacting species can equalize concentration differences. The loss mechanism is called concentration overpotential η_{conc} (Eq. 3.32).

$$\eta_{\text{conc}} = \frac{RT}{nF} ln\Big(\frac{c_{\text{s}}}{c_{\text{B}}}\Big) = \frac{RT}{nF} ln\Big(1 - \frac{i}{i_{\text{lim}}}\Big) \tag{3.32}$$

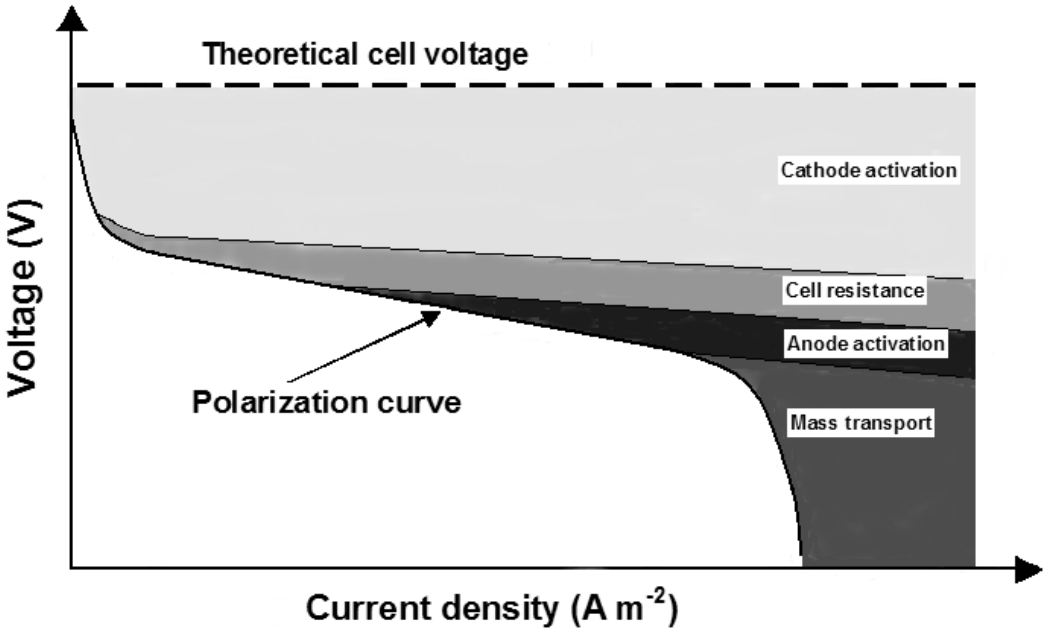

Figure 3.2: The shape of a typical polarization curve for the PEFC and the DMFC.

where c_{s} and c_{B} are the surface and the bulk concentrations of the reactants, respectively. The activation overpotential η_{act} and concentration overpotential η_{conc} exist at both electrodes and the total overpotential at the anode and the cathode can be defined according to Eqs. 3.33 and 3.34.

$$\eta_{\mathrm{a}} = \eta_{\mathrm{act,a}} + \eta_{\mathrm{conc,a}} \tag{3.33}$$

$$\eta_{\mathrm{c}} = \eta_{\mathrm{act,c}} + \eta_{\mathrm{conc,c}} \tag{3.34}$$

The overpotential increases and decreases the electrode potential at the anode and the cathode, respectively. As a result, the total cell voltage decreases. The actual cell voltage V_{cell} can be calculated by subtracting the overpotentials at the electrodes and the total resistive losses of the cell from the potential difference between the electrodes:

$$V_{\mathrm{cell}} = E_{\mathrm{c}} - E_{\mathrm{a}} - |\eta_{\mathrm{c}}| - |\eta_{\mathrm{a}}| - iR \tag{3.35}$$

The actual DMFC performance can be investigated by measuring the polarization curve. The shape of a typical polarization curve for the PEFC and the DMFC is presented in Fig. 3.2 and the effects of the different loss mechanisms are also marked in the same figure. The current density i at the electrodes can be calculated according to the *Butler-Volmer equation*:

$$i = i_0\Big(exp\big(\frac{\alpha_\mathrm{a}F}{RT}\eta_\mathrm{a}\big) - exp\big(-\frac{\alpha_\mathrm{c}F}{RT}\eta_\mathrm{c}\big)\Big) \tag{3.36}$$

When assuming high overpotentials and relatively slow kinetics at one electrode compared to the other electrode, the first or second term in Eq. 3.36 can be neglected. Thus, the current production at the cathode and the anode can be described by the *Tafel equation* (Eqs. 3.37 and 3.38, respectively).

$$i_\mathrm{c} = -i_0^\mathrm{c}\, exp\Big(-\frac{\alpha_\mathrm{c}F}{RT}\eta_\mathrm{c}\Big) \tag{3.37}$$

$$i_\mathrm{a} = i_0^\mathrm{a}\, exp\Big(-\frac{\alpha_\mathrm{a}F}{RT}\eta_\mathrm{a}\Big) \tag{3.38}$$

At low overpotentials, the anodic current production can be approximated with the linearized *Butler-Volmer equation* (Eq. 3.39).

$$i_\mathrm{a} = i_0^\mathrm{a}\,\frac{\alpha_\mathrm{a}F}{RT}\eta_\mathrm{a} \tag{3.39}$$

4 Proton Conducting Membranes for the DMFC

4.1 General

Different kinds of membrane properties are required for different applications, e.g. low MeOH permeability is favourable for the DMFC. Other desired properties are high proton conductivity (low area resistance), good dimensional and chemical stability, sufficient mechanical strength, good compatibility with the electrode and long durability (life time) in the DMFC. Altogether, the development work of DMFC membranes is a complex optimization problem due to numerous interrelated parameters, e.g. an increase of conductivity often weakens the mechanical and chemical properties of the membrane and thus decreases the life-time in the fuel cell.

In this thesis, four different membranes for the DMFC are investigated: commercial Nafion® as a reference material, ETFE-SA (sulphonated poly(ethylene-*alt*-tetrafluoroethylene)), PVDF-*g*-PSSA (poly(vinylidene fluoride)-*graft*-poly(styrene sulphonic acid)) and sPSO2 (sulphonated poly(phenylene sulphone)) membranes. The main properties of the investigated membranes are presented in Table 4.1 and the chemical structures in Fig. 4.1. It can be seen that the structures and properties of the membranes differ significantly from each other, but the common thing is that all investigated membranes contain highly polar and hydrohilic sulphonic acid

Table 4.1: The main properties of the investigated membranes.

	l_{dry} (μm)	l_{wet} (μm)	WU (%)	d.o.g. (%)	IEC (meq g^{-1})	σ (25 °C) (mS cm^{-1})	R_A (25 °C) ($\mu\Omega$ m^2)
Nafion® 117	180	210	20	–	0.9	50	42
ETFE-SA	35	40	11	–	1.4	10	40
PVDF-*g*-PSSA	70	90	85	39	2.5	45	20
sPSO2	60	90	115	–	2.3	130	7

groups SO_3^-, which enable proton conductivity of the polymers. The proton conductivity of the DMFC membranes used nowadays is based on water sorption and the resistance of the membrane is a major contributor to the total ohmic loss of the cell [86]. In practice, the conductivity is high enough for many applications, but the operation range is limited to temperatures below 100 °C. Besides the temperature, the proton conduction depends also on the structure of the polymer, its degree of hydration, pressure and concentrations of other species, e.g. MeOH molecules [86]. The actual proton transport in proton conducting membranes takes place with both a *Grotthuss mechanism*, i.e. structure diffusion (or proton hopping) and a *vehicle mechanism*, i.e. matrix transport [35,86]. Because the thicknesses of the membranes vary quite much, the area resistance R_A (Eq. 4.1) describes the actual DMFC performance better than conductivity.

$$R_\mathrm{A} = RA = \frac{l}{\sigma} \tag{4.1}$$

where l is the thickness of the membrane. Because the R_A is directly proportional to l, the ohmic losses can be decreased by decreasing the thickness of the membrane. As a drawback, the MeOH crossover rate increases when the membrane is thinner. The membrane conductivity and the ohmic losses of the fuel cell can be measured e.g. with AC impedance spectroscopy [96–100]. Also, many membrane properties depend on the *ion exchange capacity* (IEC), which is related to the amount of sulphonic acid groups in the membrane:

$$IEC = \frac{n_\mathrm{acid} z_\mathrm{acid}}{m_\mathrm{mem}} = \frac{n_{\mathrm{SO}_3^-}}{m_\mathrm{mem}} = \frac{1000}{EW} \tag{4.2}$$

where m_mem is mass of dry membrane, $n_{\mathrm{SO}_3^-}$ is the amount of sulphonic acid groups and EW is equivalent weight of the membrane. Typically for the DMFC membranes IEC is 1-3 meq g^{-1} (for monovalent substances meq g^{-1} = mmol g^{-1}). The water uptake WU of a membrane is determined according to Eq. 4.3:

$$WU = \frac{m_\mathrm{mem}^\mathrm{wet} - m_\mathrm{mem}^\mathrm{dry}}{m_\mathrm{mem}^\mathrm{dry}} \times 100\% \tag{4.3}$$

Nafion®

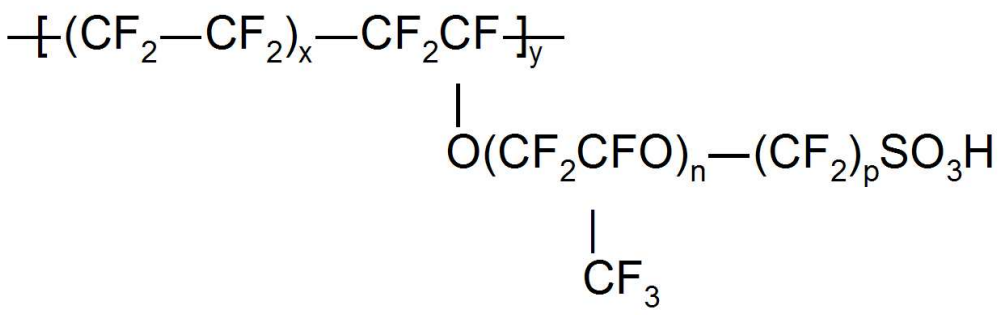

ETFE-SA

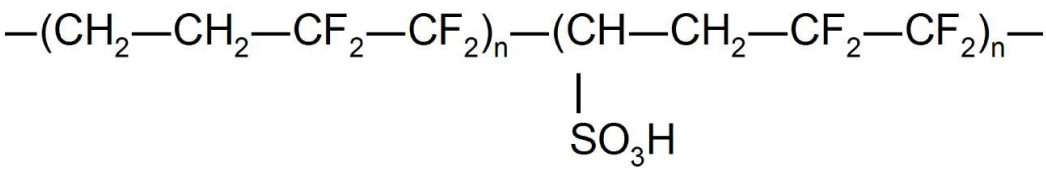

PVDF-*g*-PSSA

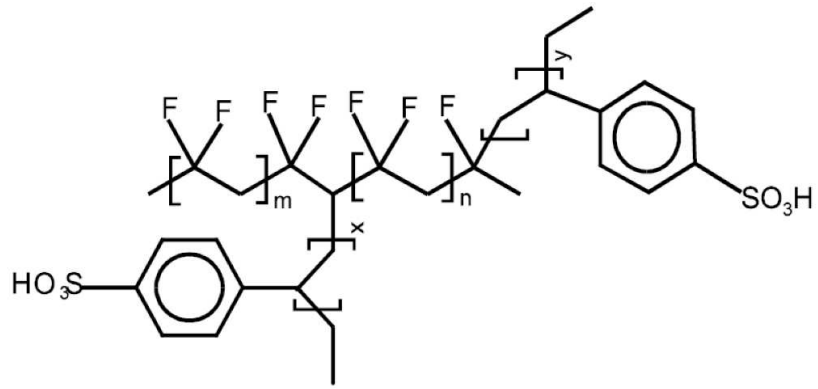

sPSO2

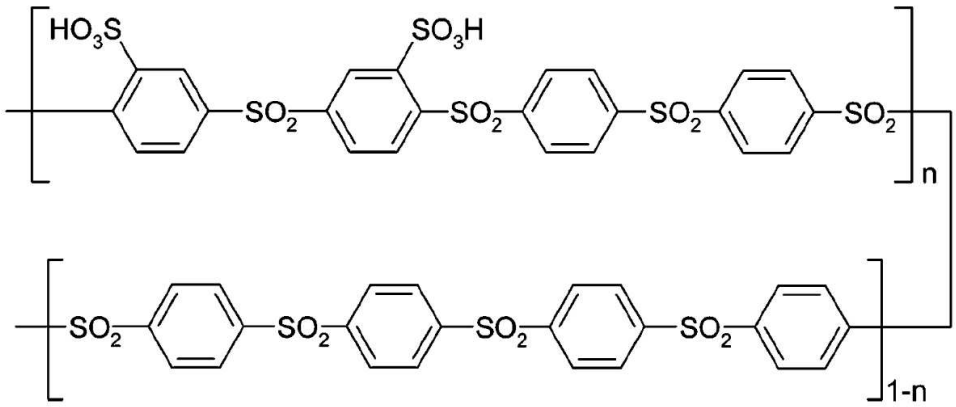

Figure 4.1: Chemical structures of the investigated membranes.

4.2 Perfluorosulphonated Nafion® Membranes

The very first investigations concerning the Nafion® membrane by E. I. du Pont de Nemours and Company have already been done as early as in 1962 [9] and ever since its development work has continued over four decades [101–103]. Nafion® is a copolymer of tetrafluoroethylene (TFE) and perfluoro(4-methyl-3,6-dioxa-7-octene-1-sulphonyl fluoride) or "vinyl ether" [104]. Nafion® and similar derivatives are fully fluorinated and therefore, they do not suffer from rapid degradation in a fuel cell, because C–F bonds are more stable than C–H bonds [8].

The perfluorinated composition of the Nafion® copolymer imparts chemical and thermal stability rarely available in non-fluorinated polymers [104]. The ionic functionality is introduced in preparation, when sulphonyl fluoride groups (SO_2F) are chemically converted to sulphonic acid (SO_3H). The copolymer's acid capacity is related to the relative amounts of co-monomers specified during polymerization and can range from 0.67 to 1.25 meq g^{-1} (1500-800 EW, respectively) [104]. Altogether, the manufacturing process of the Nafion® membrane consists many steps and is quite complicated and time consuming. Naturally, this affects also the price of the final product. The preparation and properties of Nafion® are well described in the literature, see e.g. review articles of Souzy *et al.* [7], Mauritz *et al.* [105] and Doyle *et al.* [106] and Refs. therein.

There are also some other manufacturing processes for the sulphonated tetrafluorethylene copolymers, which structure, i.e. the length of polymer side chain, differs from the Nafion® membrane. The best known alternatives are the Dow® membrane by Dow Chemical Company [107–109], the Flemion® membrane by Asahi Glass Company [110–112] and the Aciplex® membrane by Asahi Chemicals [113, 114]. The chemical structure of Nafion® (in protonic form) is presented in Fig. 4.1 (n = 1, x = 5-13.5, p = 2). As a comparison, for Dow® n = 0, x = 3.6-10, p = 2, for Flemion® n = 0-1, p = 1-5 and for Aciplex® n = 2, x = 1.5-14, p

= 2-5 [7]. The perfluorosulphonated membranes have a relatively good conductivity (30-100 $\mathrm{mScm^{-1}}$) [34, 115, 116], but the drawback is their high methanol permeability [117, 118]. The Nafion® 117 membranes have also been widely used in the DMFC studies, e.g. [34, 89, 119–125], because they have the lowest MeOH crossover rate of the commonly used Nafion® membranes [125].

In this thesis, the Nafion® 117 membranes are used as a reference material in most of the studies. The first two numbers after Nafion® are the equivalent weight of the membrane (EW) divided by 100 (EW = 1100 g $\mathrm{Eq^{-1}}$) and the last number describes the nominal dry thickness of the membrane in mils (1/1000 of an inch). Thus for Nafion® 117 $l_{\mathrm{dry}} = 7 \times 2.54 \times 10^{-5}$ m = 180 μm. The thinner Nafion® membranes i.e. Nafion® 112 (l_{dry} = 50 μm) and Nafion® 115 (l_{dry} = 130 μm) are also used in some studies of this thesis.

4.3 Irradiated and Direct Sulphonated ETFE-SA Membrane

Most of the investigations included in this thesis are done with the direct sulphonated poly(ethylene-*alt*-tetrafluoroethylene) (ETFE-SA) membrane and its characterization has been closely connected to its development process. An attractive aspect of the ETFE-SA membranes is that they are substantially cheaper (30-100 $\$/\mathrm{m^2}$) than the membranes based on poly(perfluorosulphonic acid) (500-2000 $\$/\mathrm{m^2}$). During the manufacturing process, the properties of the ETFE-SA membrane (e.g. conductivity, water uptake, mechanical properties) can be controlled indirectly by adjusting the parameters related to irradiation and sulphonation treatment. The irradiation treatment causes crosslinking of the ETFE polymer chains, which affects the properties of the membrane. Typically uncrosslinked membranes have higher water uptake and conductivity, but their stability is quite poor. The crosslinked membranes are brittle rather than rubbery and have higher stability, but on the other hand, lower water uptake and conductivity.

The ETFE-SA membrane is made of commercial 30 μm thick poly(ethylene-*alt*-tetrafluoroethylene) (ETFE) film by irradiation followed by direct sulphonation (no grafting). The ETFE film is irradiated with a proton beam with the total dose of 500 kGy and dose rate of 2.7 kGy s^{-1} to activate the film for a functionalization reaction. The films are kept in a high vacuum (10^{-6}-10^{-5} Pa) and at temperatures below -70 °C during the irradiation. After irradiation the films are stored in liquid nitrogen. The irradiated films are then sulphonated and the sulphonic acid groups are bound directly to the polymer backbone. A tentative structure of the ETFE-SA membrane is presented in Fig. 4.1.

4.4 Radiation-Grafted PVDF-g-PSSA Membrane

The radiation grafting method has been invented over 40 years ago and is based on electromagnetic (electrons, gamma or X-rays) or proton irradiation of a suitable polymer film. The method is described in detail in Refs. [126–129] and many different kinds of radiation-grafted membranes have been developed during the years [36, 130, 131]. Because of the cheap base material, it is a very cost effective manufacturing method for the fuel cell membranes. Due to the flexibility of the preparation technique, membrane characteristics such as ion exchange capacity, water uptake and proton conductivity can be controlled with the manufacturing parameters [132]. As only a few preparation steps are required and the processing of the polymer into a membrane can be avoided, the irradiation grafting methods offer advantages in terms of economic feasibility, and remain of great interest as a route to new, less expensive polymer electrolyte membranes [132].

The PVDF-*g*-PSSA membrane investigated in this thesis is made of poly(vinylidene fluoride) film by an irradiation method followed by grafting with styrene monomers. The amount of the grafted polystyrene can be controlled by careful choice of the grafting conditions. After grafting the material is sulphonated in chlorosulphonic acid / dichloroethane solution. Chlorosulphonic acid reacts with the aromatic rings

of polystyrene and results in the formation of the PVDF-*g*-PSSA membrane, the tentative chemical structure of which is presented in Fig. 4.1. The detailed manufacturing process and many properties of the PVDF-*g*-PSSA membrane have already been reported in Refs. [132–138]. The degree of grafting (*d.o.g.*) is determined according to Eq. 4.4:

$$d.o.g. = \frac{m_{\mathrm{graf}} - m_0}{m_0} \times 100\% \tag{4.4}$$

where m_0 and m_{graf} are the masses of the polymer film before and after grafting. The degree of grafting of the PVDF-*g*-PSSA membrane used in this study is 39% and the conductivity is quite equal to Nafion® 117, which is much thicker than PVDF-*g*-PSSA (see Table 4.1). Even higher conductivities (up to 80 mS cm^{-1} at 20 °C) have been reported [135] for PVDF-*g*-PSSA with higher *d.o.g.* values, but with decrease in mechanical and chemical properties of the membrane. The long-term stability of the PVDF-*g*-PSSA membrane in the PEFC has been investigated by Kallio *et al.* [139] and both the general loss of PSSA and accelerated degradation at the cathode side of the membrane has been observed under fuel cell conditions.

It has been observed [116, 140–142] that typically the rate of degradation of styrene grafted and sulphonated membranes in the PEFC is clearly higher than that of Nafion®. This has been explained mainly by the chemical instability of the polystyrene sulphonic acid. However, there have also been some indications of the correlation between the rate of degradation and water uptake [116] so that membranes with higher water uptakes, e.g. PVDF-*co*-HFP(15%)-*g*-PSSA and FEP-*g*-PSSA, have been reported to crack quickly in the PEFC. Also, the ETFE has proved to be a stable matrix polymer for the radiation grafted membranes, e.g. ETFE-*g*-PSSA has survived longer compared to PVDF-*g*-PSSA in the PEFC and no crack formation has been observed [116].

4.5 Sulphonated Poly(arylene) sPSO2 Membrane

Poly(arylene) based membranes [38, 40, 143] are also an attractive alternative for PEFC and DMFC membranes, because of their low MeOH crossover and both higher T_g and tensile strength compared to perfluorosulphonic acid polymers [143]. The only hydrocarbon membrane included in this study is a sulphonated poly(phenylene sulphone) (sPSO2) membrane with a particularly high IEC of 2.3 meq g^{-1}. The tentative structure of the sPSO2 membrane is presented in Fig. 4.1. In the sPSO2 membrane, an aromatic ring bearing the sulphonic acid group is bound to two strongly electron-withdrawing sulphone groups (-SO_2-).

The sPSO2 membrane is made by a two-step process comprising (1) a nucleophilic aromatic polycondensation reaction of 4,4'-difluorodiphenylsulphone and disodium 3,3'-disulphonate-4,4'-difluorodiphenylsulphone with 4,4'-thiobisbenzenethiol resulting in sulphonated poly(phenylene sulphide sulphone)s and (2) their subsequent oxidation using peroxide in acidic solution [143]. The very first sPSO2 membranes have been synthesized recently and in this thesis, only swelling and fractionalization experiments for the sPSO2 are included. Preparation, characterization and other properties of sPSO2 membranes are described in detail by Schuster *et al.* [143].

The sPSO2 membranes, which have electron-deficient aromatic rings, show high thermal, thermo-oxidative and hydrolytic stability, low solubility and reduced swelling in water at enhanced temperatures compared to other sulphonated poly(arylene)s [143]. The conductivity of sPSO2 is very high, but the main challenges of this membrane are related to its mechanical properties and compatibility with the DMFC electrodes.

5 Experimental and Computational Methods

5.1 General

An extensive membrane characterization is important for membrane development, because there are numerous interconnected parameters, which all affect membrane properties and the actual performance in the fuel cell. The membrane characterization and measuring the key parameters is fundamental work for novel membranes, which is described in detail in Publications I-III of this thesis. The commercial Nafion® membranes are used as reference material in all studies, because their properties are quite well known and they have been investigated worldwide for over 30 years.

The characterization enables the comparison between different alternative membranes and also some preliminary predictions concerning the actual DMFC performance can be given. It also enables a good control of the manufacturing process of the membranes, e.g. controls the quality of the membranes and ensures their homogeneity. Altogether, combining the information gained with different techniques can be considered substantial for a systematical approach to membrane development. Naturally, fuel cell tests are also needed, because it is important to know how membranes operate as part of a DMFC under various operating conditions, e.g. the surface properties of the membrane determines its compatibility with the electrodes and affects mass transport of the reacting species towards and away from the electrodes.

The long-term stability under different DMFC conditions gives vital information for practical applications. Those investigations are described in detail in Publication I of this thesis. The current distribution measurements (Publication IV) are also very valuable for better understanding of the complex relationships between different variables and operation parameters of the DMFC, which is especially true in the

case of the free-breathing DMFC. The current distribution at the electrodes gives indirect information on local concentrations of reacting species and mass transfer phenomena occurring inside the DMFC. In order to investigate the MeOH crossover and other mass transfer phenomena more profoundly, a three-dimensional model is also developed for the free-breathing DMFC (Publication V). The model validations are done using the experimental results obtained from the current distribution measurements. The developed model enables that different kinds of mass transfer phenomena and e.g. local concentrations of the reacting species can be investigated computationally.

5.2 Surface Analysis

It is important to know the surface properties of the membranes, because the surface morphology is assumed to affect also the membrane performance in the fuel cell [140, 144, 145]. An atomic force microscopy (AFM) is widely used, when the surface morphology of membranes is investigated [146–148]. The AFM imaging is based on the surface forces between the tip and the substrate. The tip is held in a cantilever, the movements of which are recognized with a laser beam reflecting off the cantilever [149]. In this thesis, the surface morphology and also the morphology changes originating from swelling are investigated with the AFM.

The AFM device used in Publication II of this thesis is a Explorer^{TM} Scanning Probe Microscope Model TMX 2000 (TopoMetrix GmbH) with AFM electrochemistry probes (P/N 1710-00). In order to get an AFM image from the surface of the dry membrane, the surface is scanned (in non-contact mode) with an Explorer^{TM} AFM Dry Scanner. When the swelling properties of the membranes are investigated, the AFM images are taken with an Explorer^{TM} AFM Liquid Scanner, because the Liquid Scanner can also be used with dry samples. The following AFM imaging procedure has been used during the swelling experiments: The first AFM image is taken from the surface of the dry membrane. Then a water droplet is introduced

and after that the surface scans are repeated from the same location as a function of time. During those scans the probe is completely inside the water droplet.

Detailed structural information of the membranes can also be obtained with a scanning electron microscope (SEM). The SEM is a very convenient tool for the investigations of surface properties of membranes and porous electrodes. Unlike the transmission electron microscope (TEM), where the electrons are detected by beam transmission, the SEM produces images by detecting secondary electrons, which are emitted from the surface due to excitation by the primary electron beam. The SEM images presented in Publication II are taken with a Hitachi S-4800 field emission scanning electron microscope with an acceleration voltage of 1 kV and operation distance of 4 mm. Prior to imaging, the samples are coated with a 4 nm thick platinum layer.

Scanning electrochemical microscopy (SECM) is a technique, which can be used for a wide variety of electroanalytical studies [150–152]. In Publication II of this thesis, the SECM is used to study surface morphology and proton concentration variations on the surface of the membrane. The measurements are done with a SECM model CHI-900 (CH Instruments). Before doing the measurements the membranes are equilibrated with a solution of 10^{-3} M HCl (Riedel-deHaên) and 0.1 M KCl (Merck) for a minimum of three days changing the salt solution to a fresh one daily. The KCl salt is used in the solution as a supporting electrolyte. Prior to the measurements the cell is deoxygenated by purging with N_2 and also during the measurements the gas phase in the cell is continuously flushed with N_2.

During the SECM measurements the membrane is fixed horizontally in a two-compartment cell on a porous glass sinter to keep the membrane wet and to prevent it from deforming when the surface is contacted by the SECM tip. The cell is filled with the above-mentioned KCl - HCl solution. The SECM tip (working electrode) is made of 25 μm thick platinum wire sealed in glass. The detailed manufacturing

method of the working electrode is described in Ref. [153]. A silver wire is used as a combined reference and counter electrode. If the surface of the membrane is inhomogeneous with respect to proton availability, the reactivity of the surface can be studied from the current response at the SECM tip. The magnitude of the current depends on differences in the chemical structure of the membrane surface and also the distance between the tip and the membrane.

Surface scans (200 $\times$ 200 μm) are obtained by setting the SECM tip potential to mass transport limited region for proton reduction and keeping it constant during the mapping. The current of the tip is then recorded as a function of its position. The scanning is made with a speed of 25 μm s^{-1} at a distance of 5 μm from the surface of the membrane. Above the more conductive regions the current is higher than the bulk current, whereas above the more insulating regions, it is lower. A similar experimental setup is described in Ref. [152].

The hydrophilicity of the membrane surface can be an important factor in determining water uptake characteristics, which would be expected to influence the proton conductivity and thus, also fuel cell performance [154]. The surface hydrophobicity/hydrophilicity is investigated in Publication II of this thesis with a water contact angle (CA) measurement. The measurements are carried out with a goniometer (CAM 100, KSV Instruments) at 25 °C (Fig. 5.1). The sample is put on a sample table and a droplet of water is placed on the sample with a syringe. Immediately after introducing the droplet, 10 images are taken of the droplet with a digital camera during 10 seconds and a curve is fitted to the edge of the droplet in the image.

From the fitted curves the CA values can be calculated as a mean value. The lower and higher CA values refer directly to the lower and higher surface hydrophobicities, respectively. In order to investigate how the irradiation treatment followed by sulphonation affected the surface hydrophobicity/hydrophilicity properties, different kinds of samples are investigated with the CA method: an untreated ETFE film,

Figure 5.1: The goniometer used in water contact angle (CA) measurements.

an ETFE-SA membrane with a low degree of sulphonation and another ETFE-SA membrane with a higher degree of sulphonation. Here the high degree of sulphonation refers to the sulphonation level, which is adequately high for a good proton conductivity and efficiency in the DMFC. The low degree of sulphonation refers to a substantially lower amount of sulphonic acid groups in the membrane. The CA measurements are done for both sides of the membranes and at several locations.

5.3 Structural Analysis

A thorough structural analysis of the membranes is required to assure an adequate thermal and mechanical stability for their use in the DMFC. In addition, the structural differences originating from the manufacturing process can be investigated and membrane specific properties can be determined. The thermal stability of the initial ETFE film and the ETFE-SA membrane are studied in Publication II with thermogravimetric analysis (TGA) (Mettler Toledo TGA 850) under N_2 atmosphere. The sample is placed in a 70 μl aluminium oxide crucible and heated from 25 °C to 600

°C with a heating rate of 10 °C min^{-1}. During heating the mass loss of the sample is detected.

The glass transition temperature T_g of membrane materials is measured using a dynamic mechanical analysis equipment (DMA Q800, TA-instrument). The DMA measurements in Publication II are done in the tensile mode at an oscillation frequency of 1 Hz. The dimensions of the test film are approximately 7 mm long × 4 mm wide × 30 μm thick. A sinusoidal amplitude strain of 30 μm is applied during the temperature sweep from -50 °C to 300 °C at a rate of 3 °C min^{-1}. The value of T_g is evaluated from the loss tangent $\tan\delta$ curve as the maximum of the peak according to Eq. 5.1.

$$tan\,\delta = \frac{E''}{E'} \tag{5.1}$$

where E'' is loss modulus and E' storage modulus of the membrane. The elementary profiles along the membrane cross-section are analyzed in Publication II with a Zeiss DSM 962 scanning electron microscope combined with a Link Isis energy dispersive X-ray spectrometer (EDX). Membranes are placed between metal plates and the cross-section is cut with a razor blade. The elementary analysis is then made along the cross-section line.

When the elementary analysis is done for the ETFE-SA membrane with the EDX, the most interesting element is sulphur. The sulphur profile along the cross-section of the ETFE-SA membrane gives information about the distribution of sulphonic acid groups and consequently the information about the success of the sulphonation process can be obtained. That information is important for adjusting the optimal sulphonation parameters, as a part of development work of membranes. Walsby *et al.* [155] have used a similar method for investigations concerning sulphonation processes of the different styrene grafted fluoropolymer films.

5.4 Swelling and MeOH Permeability

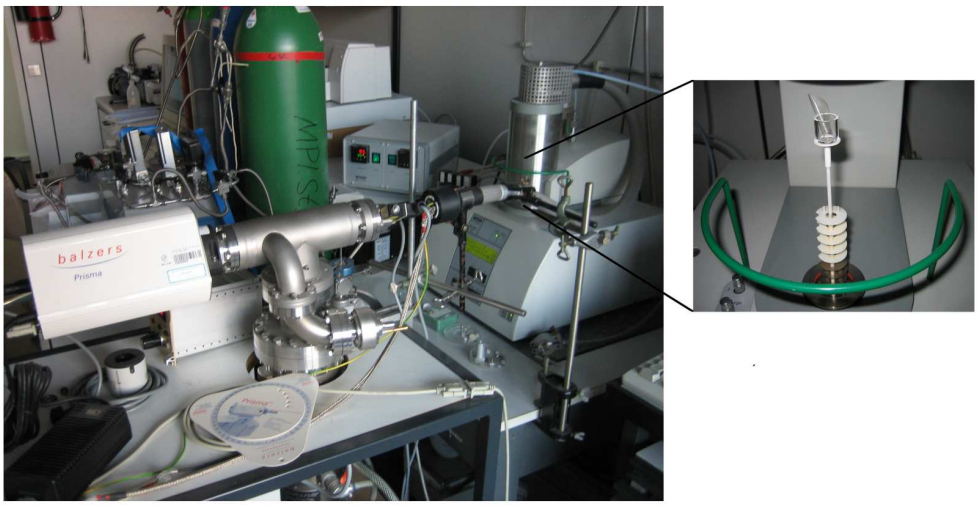

Figure 5.2: The combined thermogravimetry and mass spectrometer used in this thesis.

Understanding of the nature of swelling is considered to be essential for the development of optimized membranes for the DMFC. Especially, it is important to know swelling properties in water - MeOH solutions, but in order to investigate wider the swelling process, the swelling experiments are also done in higher alcohol (EtOH, 2-PrOH, *t*BuOH) - water and H_2SO_4 - water mixtures. The swelling and fractionalization experiments presented in Publication III of this thesis are concentrated on the ETFE-SA, the PVDF-*g*-PSSA and the Nafion® membranes, but some experiments are also done for the sPSO2 membrane. There are already many reports on the total solvent uptake of diverse membranes in MeOH - water mixtures [90, 156–159] and some other solvents [160, 161], but selectivity studies are scarce.

Any selectivity of the solvent uptake from water - MeOH mixtures is of importance for the performance of the membranes in the DMFC. Thus, both the total swelling in mixtures of water and diverse alcohols as a function of water / alcohol ratio

and the selectivity of the solvent uptake for different membranes are investigated. Qualitative rationales are also given explaining the distinct differences in swelling behaviour and selectivity with respect to water / methanol uptake. The liquid uptake (LU) and water / alcohol selectivity (S) values are determined in Publication III by thermal desorption using combined thermogravimetry (TG) (NETZSCH STA 449C thermobalance) and mass spectrometer (MS) (Balzers Prisma quadrupol spectrometer), which are shown in Fig 5.2. This allows to determine the total solvent uptake and the alcohol - water fractions inside the membranes compared to the corresponding water - alcohol fractions of the solutions. For H_2SO_4 - water mixtures, only the total liquid uptake is measured.

Prior to experiments the membranes are equilibrated in water - alcohol mixtures for 3-7 days at room temperature. Before transferring the samples into the TG, the adhering liquid is quickly swept away. The samples are heated with a rate of 5 °C min^{-1} from 25 to 135 °C and kept at least 15 min at this temperature in order to ensure complete solvent desorption. The signals detected by the MS are calibrated with respect to the signals obtained in evaporation experiments of the corresponding water - alcohol mixtures. The LU values can be calculated according to Eq. 5.2:

$$LU = \frac{m_{\mathrm{mem}}^{\mathrm{wet}} - m_{\mathrm{mem}}^{\mathrm{dry}}}{m_{\mathrm{mem}}^{\mathrm{dry}}} \tag{5.2}$$

The selectivity S of the solvent uptake is calculated according to Eq. 5.3:

$$S = \frac{n_{\mathrm{H_2O}}^{\mathrm{mem}}}{n_{\mathrm{MeOH}}^{\mathrm{mem}}} \times \frac{n_{\mathrm{MeOH}}^{\mathrm{sol}}}{n_{\mathrm{H_2O}}^{\mathrm{sol}}} \tag{5.3}$$

The MeOH permeability through the membrane, i.e. MeOH crossover in the DMFC, is closely connected to the swelling and fractionalization properties of the membrane. The permeability is mainly determined by the microstructure of the membrane, which is the result of a constrained hydrophobic / hydrophilic separation and the degree of swelling [34]. There are different kinds of methods to measure MeOH permeability through the DMFC membranes [89, 162–165] and in this thesis, the MeOH permeability is investigated with both a diffusion cell (Publication II) and

in real DMFC conditions (Publication I). In the first method, the MeOH diffusion through the membrane is measured using a diffusion cell containing two stirred compartments separated by the membrane: one filled with deionized water and the other with a 15 M MeOH solution. The measurements are done at three different temperatures (30, 50 and 70 °C) and during the temperature of the diffusion cell is controlled with a water bath. The MeOH permeability P is calculated according to Eq. 5.4, which is described in detail in Ref. [163].

$$P = \frac{DH}{l} = \left(\frac{V_{\mathrm{H_2O}} \times V_{\mathrm{MeOH+H_2O}}}{At(V_{\mathrm{H_2O}} + V_{\mathrm{MeOH+H_2O}})} \right) ln \left(\frac{c^0_{\mathrm{H_2O}} - c^0_{\mathrm{MeOH+H_2O}}}{c_{\mathrm{H_2O}} - c_{\mathrm{MeOH+H_2O}}} \right) \tag{5.4}$$

where D is diffusion coefficient, H is partition coefficient, l is thickness of the membrane, A is cross-section area (0.7 $\mathrm{cm^2}$), t is time, V is compartment volume (3.7 $\mathrm{cm^3}$), c is MeOH concentration (wt-%), superscript 0 is for initial condition, subscript 'MeOH+H_2O' refers to the compartment, which is originally filled with 15 M methanol and subscript 'H_2O' to the compartment originally filled with deionised water. A 30 μl sample is taken from a compartment and then mixed with a 10μl reference sample (0.5 M 1,4-dioxane). Furthermore, a 2 μl sample is taken from that 40 μl sample and injected to a gas chromatography system (HP 6890 with HP-5 Siloxane column) in order to determine MeOH concentration.

The other method used to evaluate the MeOH permeability ($\mathrm{D_{MeOH}c_{MeOH}}$) has been introduced by Ren *et al.* [89]:

$$D_{\mathrm{MeOH}} = \frac{k^2_{\mathrm{dt}}}{k^2_{\mathrm{dl}}} \frac{i^2_{\mathrm{lim}}}{[i_{\mathrm{t}}\sqrt{t}]^2_{\mathrm{Cot}}} \frac{l^2}{\pi} \tag{5.5}$$

$$c_{\mathrm{MeOH}} = \frac{k_{\mathrm{dl}}}{k^2_{\mathrm{dt}}} \frac{[i_{\mathrm{t}}\sqrt{t}]^2_{\mathrm{Cot}}}{i_{\mathrm{lim}}} \frac{\pi}{6Fl} \tag{5.6}$$

$$D_{\mathrm{MeOH}} c_{\mathrm{MeOH}} = \frac{1}{k_{\mathrm{dl}}} \frac{i_{\mathrm{lim}} l}{6F} \tag{5.7}$$

where l is the thickness of the membrane, i_{lim} is steady-state limiting current, $[i_{\mathrm{t}}\sqrt{t}]^2_{\mathrm{Cot}}$ is Cottrell slope, k_{dt} and k_{dl} are electro-osmotic drag correction coeffi-

cients for i_{lim} and $[i_{\mathrm{t}}\sqrt{t}]^2_{\mathrm{Cot}}$, respectively. The i_{lim} and $[i_{\mathrm{t}}\sqrt{t}]^2_{\mathrm{Cot}}$ values are measured, when well humidified nitrogen gas flows (270 ml min^{-1}) into the DMFC cathode and the potential is sweeped slowly (0.2 mV s^{-1}) or stepped from the OCV to the mass transfer limited region, respectively. The drag correction coefficients k_{dt} and k_{dl} can be calculated after the water drag coefficients $\lambda_{\mathrm{H_2O}}$ ($\mathrm{H_2O/H^+}$) are measured [89,90]:

$$k_{\mathrm{dl}} = \frac{ln(1 + 6\lambda_{\mathrm{H_2O}} X_{\mathrm{MeOH}})}{6\lambda_{\mathrm{H_2O}} X_{\mathrm{MeOH}}} \tag{5.8}$$

$$k_{\mathrm{dl}}\ e^{(6\lambda_{\mathrm{H_2O}} X_{\mathrm{MeOH}})^2 k_{\mathrm{dt}}^2/\pi}\left[erf\left(\frac{(6\lambda_{\mathrm{H_2O}} X_{\mathrm{MeOH}})k_{\mathrm{dt}}}{\sqrt{\pi}}\right) + 1\right] = 1 \tag{5.9}$$

where X_{MeOH} is the MeOH mole fraction. The water drag coefficient measurements are done with dry O_2 on the cathode side. The total H_2O flux emerging from the cathode is determined by collecting the water inside an U-tube filled with Dryerite® (W.A. Hammond Drierite Co.). The $\lambda_{\mathrm{H_2O}}$ value is then calculated by subtracting from the total H_2O flux the water fluxes emerging both from the MeOH oxidation and from the cell current [166, 167]. The MeOH crossover rate is determined by measuring the CO_2 flux using a linearized CO_2 sensor (GMM12B, Vaisala, Inc).

5.5 DMFC Testing

Even though some investigated membranes have very good or even excellent material properties, the true performance and suitability for the DMFC can only be verified with fuel cell tests. The DMFC is a quite corrosive and harsh environment for the polymer membranes, because it is simultaneously both reducing (anode) and oxidative (cathode). Also the compatibility of the membrane with the electrodes, i.e. the contact resistances between the electrodes and membrane, is in a key position, when the DMFC is operated at various temperatures and there exist e.g. thermal expansions, swelling and pressure gradients. Therefore, the long-term stability tests in the DMFC are important in order to find out the limits of the performance, the levels of mechanical and chemical degradation and how the fuel cell performance of the membrane changes as a function of time and operating temperature.

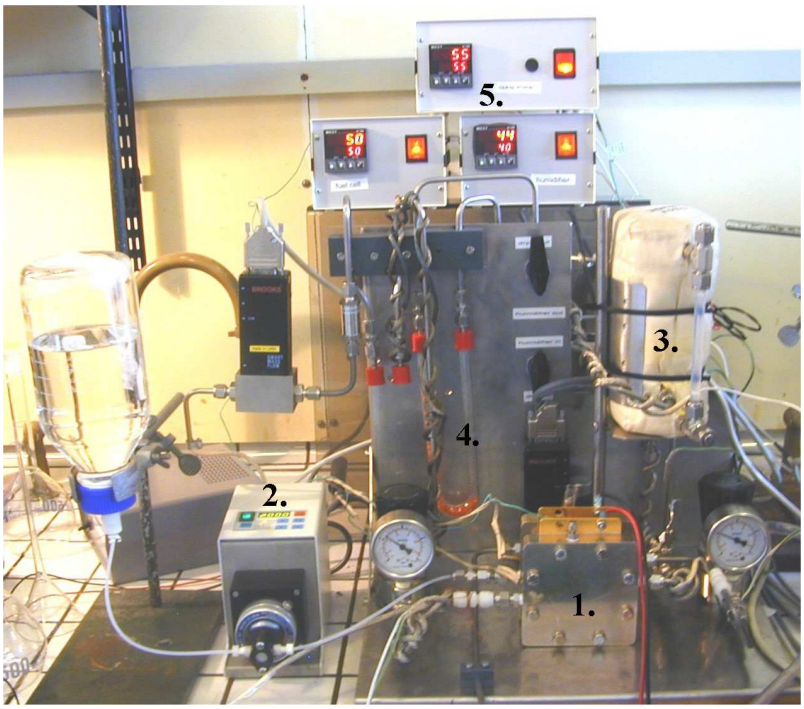

Figure 5.3: The DMFC system: 1. Fuel cell 2. MeOH pump 3. Gas humidifier 4. Gas dryer 5. Temperature controllers

The DMFC system used for membrane testing in Publication I of this thesis is presented in Fig. 5.3 and the main components are also marked in the figure. A mixture of MeOH and water is pumped with a Reglo-CPF pump (Ismatec) into the DMFC (A=5 cm^2, serpentine flow channels, Fuel Cell Technologies, Inc.). The cathode gas (oxygen/air) flow rate is controlled with a mass flowmeter (5850S, Brooks Instrument). The reactant flow rates are set to relatively high values in order to minimize mass transfer limitations at the electrodes (MeOH: 2.0 ml min^{-1}, oxygen/air: 270 ml min^{-1}). The cyclic voltammetry (CV) measurements are done at three different temperatures (30, 50 and 70 °C) with an Autolab PGSTAT20 potentiostat (Eco Chemie B.V.) with a GPES 4.8 software. Some measurements are also done in a temperature range 80-100 °C in order to find out the maximum suitable operating temperature for the ETFE-SA membrane.

During the measurements, the effects of different operational parameters are investigated: The MeOH concentration is varied on a large scale from 0.5 M to 10 M. The measurements are done both with small back pressures (cathode: 0.2 bar (g), anode: 0 bar (g)) and also with a 1 bar (g) back pressure on both compartments. The relative humidity (RH) of the different cathode gases is varied during the measurements: the reactant gas is dried in a U-tube (filled with Orange Gel) or humidified in a humidifier. The humidifier temperatures are calibrated according to the corresponding values of the gas relative humidities using a moisture meter (HMI41, Vaisala Inc.). In order to achieve the wanted RH (0-100%) inside the DMFC, the RH change is evaluated with respect to the temperature change according to the Mollier diagram for moist air. This procedure is necessary, because the gas RH can not be measured inside the DMFC flow channels. The gas tube temperature is always kept 5-40 °C above the cell temperature to prevent water condensation and the corresponding RH values inside the DMFC are calculated on the basis of the measured RH values in the gas inlet tube.

5.6 Current Distribution Measurements

In order to achieve optimum performance values for the DMFC, it is important to have an even current and temperature distribution inside the fuel cell. This can be achieved, when the concentrations of the reactants have optimum values. In many cases the goal of the fuel cell development is also to achieve an even current density profile under a variety of operating conditions. As a consequence, current distribution measurements are very valuable for better understanding of the complex relationships between different variables and operation parameters of the DMFC.

The current distribution at the cathode gives indirect information on local concentrations of reacting species and mass transfer phenomena occurring inside the DMFC. The DMFC with a segmented cathode can provide detailed information on

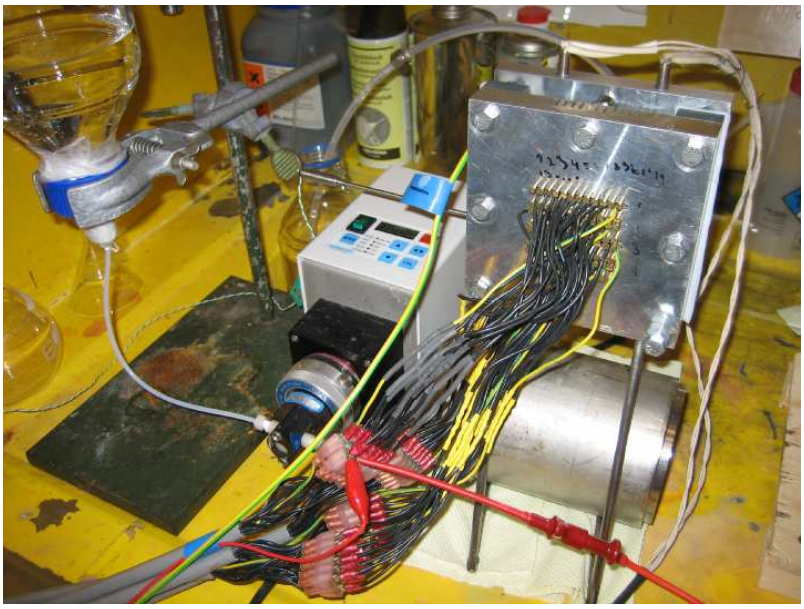

Figure 5.4: The free-breathing DMFC and the measurement system for the cathode current distribution.

local concentrations of the reacting species, on which part of the DMFC electrodes most of the current is produced and on how much the MeOH crossover phenomenon decreases the cell performance locally. During recent years, current distribution measurements have been used in many PEFC [168–177] and DMFC [119, 178–180] studies and various experimental techniques have been developed. A printed circuit board approach with segmented current collector and flow field has been used by Cleghorn *et al.* [168] and a partial membrane electrode assembly (MEA) method, where the active cathode area is varied, by Stumper *et al.* [169]. Wieser *et al.* [170] used a magnetic loop current sensor approach (Hall sensors) and Eckl *et al.* [177] a segmented bipolar plate approach.

In most of the studies the cathode has been segmented, but sometimes the anode [174, 175]. Gülzow *et al.* [119] have studied differences in different MEAs (originating from the manufacturing process) with a segmented DMFC (16 segments) and Geiger *et al.* [180] have also made segmented DMFC measurements (9 segments)

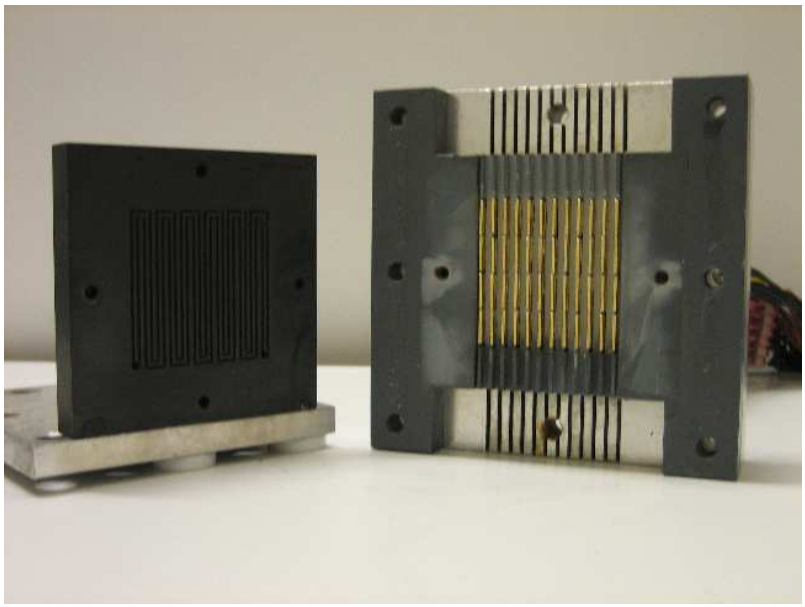

Figure 5.5: The DMFC anode flow field plate (left) and the segmented free-breathing cathode (right).

concluding that the current distribution is highly dependent on the O_2 concentration. The current distribution can also be analyzed with other data, e.g. localized impedance measurements [181], water distribution measurements [179] or distribution measurements of gaseous species (H_2O, H_2, O_2, N_2) [176]. In the catalyst studies, the array MEAs have been used as catalyst screening devices [178] and for the analysis of the local catalyst poisoning [182].

In the case of the DMFC, methanol crossover (methanol permeability through the membrane) is a very significant loss mechanism [33] and it has been investigated widely [89, 120–123, 138, 183–186]. However, most of these studies have been performed without current distribution measurements. The DMFC with a segmented cathode can provide detailed information on the concentrations of reacting species, in which part of the electrode most of the current is produced and how much the MeOH crossover phenomenon decreases the cell performance locally. All of those phenomena are not seen, if only the total cell current is measured. From the engi-

neering aspect, it is possible to see with a segmented DMFC how different MeOH flow rates affect cell performance and what is the lowest adequate MeOH flow rate (and stoichiometry), for which the performance of the DMFC is not yet MeOH mass transfer limited.

In this thesis, the main goal concerning current distribution measurements (Publications IV and V) is to investigate the mass transfer phenomena and especially MeOH crossover in the DMFC. Also, the connection between MeOH concentration and flow rate are studied in order to find their optimum values. During the measurements, the air is supplied to the cathode by free convection. The free-breathing DMFC and measurement system for the cathode current distribution is presented in Fig.5.4 and the flow field plates are presented in Fig. 5.5. The cell is aligned so that there is a free vertical convection of air upwards in the cell. The measurement system is slightly modified from the one, which is described in detail in Refs. [171,172]. In this study the cell is used as a DMFC, whereas in Refs. [171, 172] the fuel cell has been used as a PEFC with a hydrogen feed. Also the membrane electrode assemblies used are different and the anode flow field plate is designed to be more convenient for the DMFC measurements.

During the measurements presented in Publication IV the MeOH solution is pumped to the anode with a Reglo-CPF pump (Ismatec). The anode flow channel geometry is serpentine and the MeOH flow direction is mainly vertical. The segments of the cathode current collector are located against the ribs between two parallel serpentine flow channels at the anode. With that disposition the current density variations can be studied along the MeOH flow channel. The cathode flow field plate is segmented in 48 pieces: 4 horizontal rows and 12 segments in every row. The segmentation is not extended to the gas diffusion layer (GDL), only the current collector is segmented. Noponen *et al.* [171] also estimated and modelled the effect of a non-segmented GDL and concluded that the current density distribution can be measured with reasonable accuracy, even if the GDL is not segmented.

The segments are made of gold plated stainless steel and their contact force against the GDL can be individually adjusted. Every current collector pin is connected to a 0.1 Ω resistor. The current density values $i_{\mathrm{i,j}}$ can be then calculated according to *Ohm's law*. It is assumed that the effective sizes of each segments are equal ($A_{\mathrm{i,j}}$ = 25 cm^2 / 48 ≈ 0.52 cm^2). This is not exactly true, because the effective areas of the segments are slightly smaller near the edges of the cell. Also, the contacts between the pins and the GDL are not exactly equal, even though they are adjusted to be as equal as possible. The voltage drops over the resistors are measured with HP34901A multiplexer cards connected to a HP34970A data logger. During the measurements the cell is operated at steady state conditions (in constant current mode) and because only one channel is measured at a time (measurement time about 0.1 s), it takes approximately 5 seconds to measure all the segments once. The 5 s measurement sequence is followed by a 10 s rest period and the current distributions are calculated as a mean value of at least 10 sequences.

In Publication IV of this thesis, the current distribution measurements are done as a comparative study between the PVDF-*g*-PSSA and the Nafion® 117 membranes using 0.5, 1, 3, 5 and 10 M MeOH solutions and the MeOH flow rates are also varied in a wide range, from 3.3 × 10^{-9} m^3 s^{-1} to 130 × 10^{-9} m^3 s^{-1} (0.2-8 ml min^{-1}). If complete MeOH oxidation is assumed at the anode, the MeOH stoichiometry λ can be calculated according to Faraday's law of electrolysis (Eq. 5.10).

$$\lambda = \frac{nF\dot{V}c_{\mathrm{MeOH}}}{I_{\mathrm{cell}}} \tag{5.10}$$

where n is the number of electrons (6), $\dot{V}$ is MeOH flow rate and I_{cell} is measured cell current. The MeOH stoichiometry is varied in a wide range, from 3 to 2500.
The current distribution measurements are made with both PVDF-*g*-PSSA and Nafion® 117 under similar conditions. Because the cell temperature and current affect the MeOH utilization rate and the above mentioned phenomena, the measurements are done at three different cell temperatures (30, 50 and 70 °C) and using

different current densities. Most of the current measurements are done using average current densities of 120, 320 and 520 A m^{-2}. Those values are selected, because they are the most suitable to be used at all operating conditions (2 membranes, 3 cell temperatures, 5 MeOH concentrations, 3 MeOH flow rates).

5.7 Computational Methods and DMFC Modelling

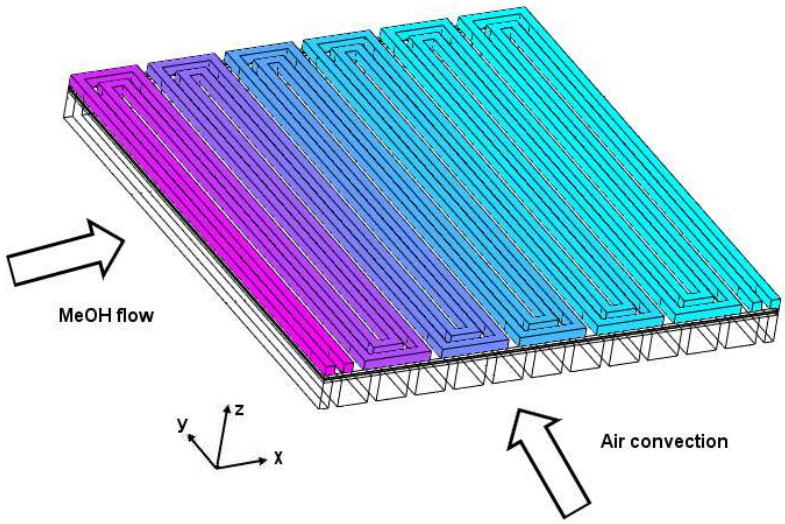

Figure 5.6: The modelled geometry and the main flow directions of reactants.

During the years, many fuel cell models for the PEFC and the DMFC have been developed, see e.g. review articles of Wang [187], Weber *et al.* [188] and Yao *et al.* [189], but most of the DMFC model validations have only been done using measured polarization curves, e.g. [189–195]. Models for passive-feed DMFCs with heat transfer effect have been set up by Chen *et al.* [196] (1D) and Rice *et al.* [192] (2D). Wang *et al.* [194] and Yang *et al.* [197] have proposed a 2D two-phase model and Danilov *et al.* [195] a 3D two-phase model of a liquid-feed DMFC. Kjeang *et al.* [198] have published a 3D model of a flowing electrolyte DMFC to simulate MeOH crossover by convection and diffusion and Liu *et al.* [199] a 3D two-phase DMFC model to investigate electron transport. Ge *et al.* [200] have made a 3D single-phase model of the DMFC to study the effects of MeOH crossover, porosities, MeOH flow rates

and channel shoulder widths.

Ju *et al.* [201] have set up a 3D PEFC model (H_2 feed) and validated it with measured current distribution data. They also concluded that model validations against only polarization curves is "insufficient and often misleading" [201]. Because the chemical reactions and connections between different operational parameters in many cases are more complicated in the DMFC than in the hydrogen fed PEFC, there is a true need for DMFC model validations using current distribution data. However, this kind of 3D model for the free-breathing DMFC has not been reported so far. Thus, a 3D model for the free-breathing DMFC is developed (Publication V) and the model validations are done according to current distribution measurements (Publication IV).

The developed model in Publication V of this thesis describes mass transfer phenomena and current production in a free-breathing DMFC, when different operation parameters as cell temperature, MeOH concentration and reactant flow rates are varied on a large scale. The model is implemented using the commercial Comsol Multiphysics 3.3 program (Comsol AB). The model is highly nonlinear and the program uses finite element method to solve the problem numerically. The model geometry is illustrated in Fig. 5.6 and the main flow directions of MeOH - water solution and free air convection are also marked in the figure. The air channels of the cell (y-axis) are vertically oriented. Implementing the DMFC model in 3D causes some restrictions and compromises to the modelling work, because the model solution should be found in a reasonable time with the available computer resources. As a comparison, much more detailed models can be implemented in 1D [191, 196], 2D [192, 194, 197] or if only some part of the DMFC, e.g. the anode [202, 203] or the cathode [204] is modelled. The following assumptions are used in the developed model:

1. Steady-state isothermal and single-phase conditions

2. No phase transitions (gas condensation or liquid vapourization) between liquid water (anode side and membrane) and water vapour (cathode side).

3. Ideal gas assumption for gaseous species and all flows are assumed to be laminar.

4. Liquid species (MeOH and water) are considered to be Newtonian fluids.

5. Complete MeOH oxidation (no partial oxidation or side reactions)

6. No gas fluxes through the membrane

7. CO_2 and H_2 fluxes are neglected.

8. All electrochemical reactions take place at indefinitely thin electrodes and no reactions occur in the membrane, porous transport layers or flow field regions.

6 Results and Discussion

6.1 Surface Properties

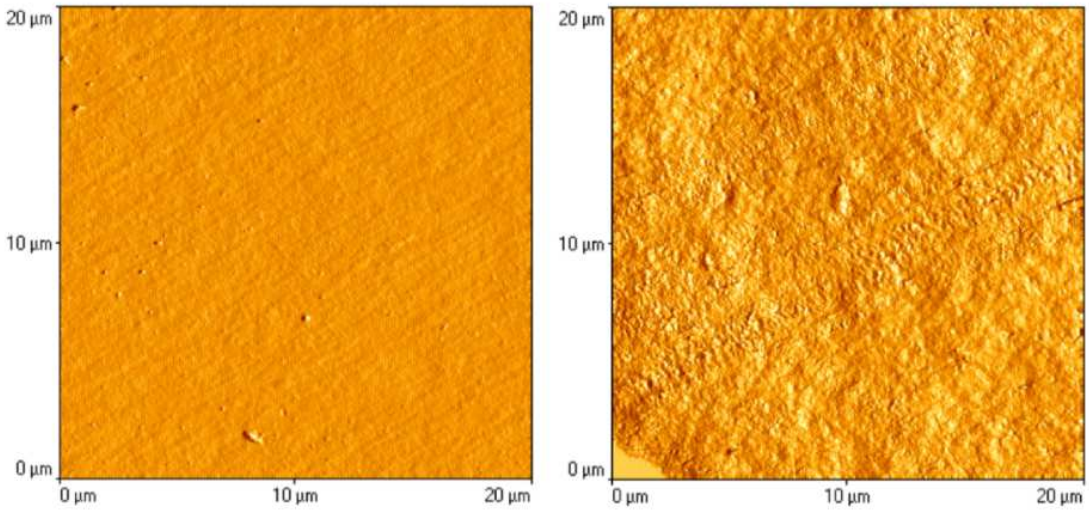

Figure 6.1: AFM images taken from the surface of Nafion® (left) and ETFE-SA (right).

When the AFM images taken from the surface of Nafion® 112, an untreated ETFE film and ETFE-SA are compared, it can be seen that the surfaces of the Nafion® 112 membrane and the untreated ETFE film are much smoother than the surface of the ETFE-SA membrane. The increased surface roughness of ETFE-SA is caused by the irradiation and sulphonation during the manufacturing process. The AFM images taken from the surface of Nafion® 112 and ETFE-SA are presented in Fig. 6.1 as a visual evidence of relatively high surface roughness of the ETFE-SA membrane. Very similar observations from the surface morphology variations can be done by comparing the images taken either with the AFM or the SEM (see Publication II).

When the ETFE-SA membranes are investigated in detail with the AFM, one can see somewhat more pores and higher roughness on that side of the membrane, which has been on the opposite side to the irradiation during the manufacturing pro-

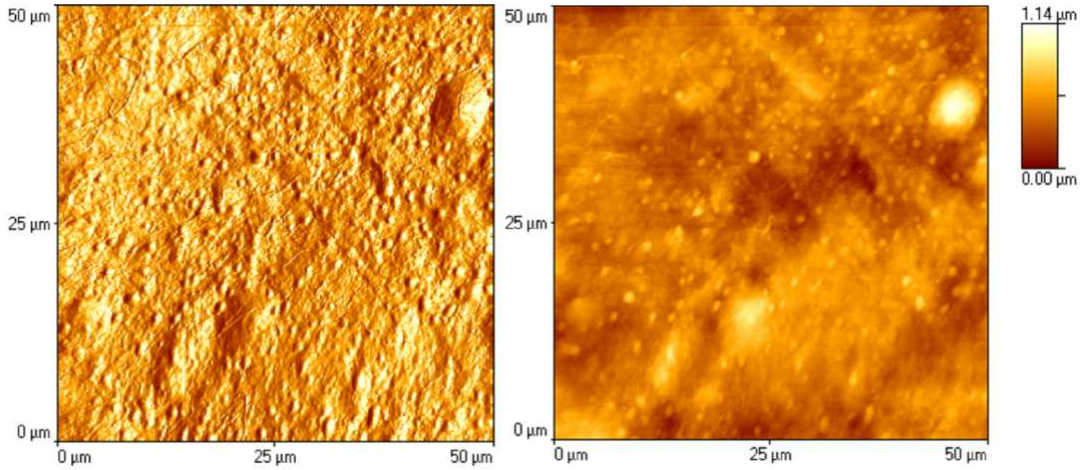

Figure 6.2: The AFM image taken and corresponding altitude profile from the surface of the ETFE-SA 15 minutes after introducing the water droplet.

cess. (The membranes have been irradiated only from the upper side.) The larger amount of pores and roughness at the bottom side is suggested to originate from back-scattering phenomena from the metal surface of the irradiation apparatus. The biggest altitude difference from hollows to bulges at the upper (irradiation) side is typically 300-400 nm and at the opposite side 400-500 nm.

Interesting swelling phenomena can be observed, when a water droplet is placed on the surface of ETFE-SA. As an example, the AFM image taken from the surface of ETFE-SA 15 minutes after introducing the water droplet is presented in Fig. 6.2. The average diameter of the swelling centers is now about 2 μm. After that swelling still continues and one can be observe relatively huge centers of swelling (diameter about 15-20 μm) after one hour. According to the swelling experiments, the Nafion® membranes have more than three times higher water uptake (WU) than the ETFE-SA membrane. As a result, when a water droplet is placed on the dry surface of the Nafion® 115 membrane, the swelling is so huge and fast that accurate AFM images are impossible to obtain with the equipment used. More AFM and SEM images of the investigated membranes are presented in Publication II of this

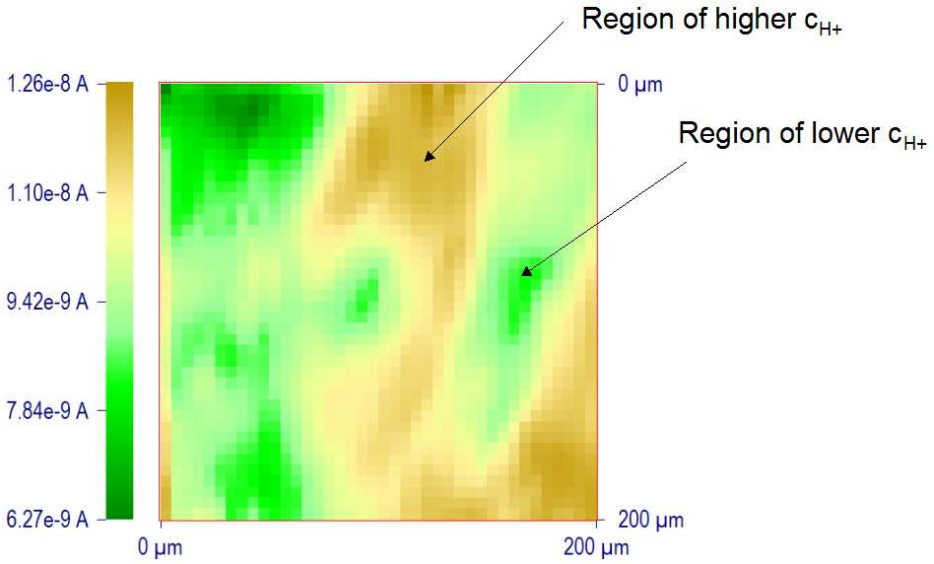

Figure 6.3: A SECM surface scan from the surface of the ETFE-SA membrane. The arrows indicate areas of higher and lower proton concentrations.

thesis.

An example of a surface scan of the ETFE-SA membrane, which is measured with the SECM, is presented in Publication II and Fig. 6.3 of this thesis. Arrows indicate areas of higher and lower proton concentrations. When these surface scans are measured from different locations of the membrane, some approximations can be done for the proton concentration variations. Even though the proton concentration data is quite non-quantitative, the different membranes can be compared. Higher variations of proton concentration refer to a more inhomogeneous material. When trying to do surface scans at a distance of 5 μm above the surface of the Nafion® 115 membrane, it is observed that the investigated surface is too soft and gelatinous for the SECM measurements. The SECM tip is stuck on the surface and contaminated. Also, when the surface scan is repeated higher above the surface, any variations in proton conductivities cannot be seen. This indicates that the surface of the Nafion® membrane is homogeneous and variations in proton conductivity are very low.

Table 6.1: The contact angles (CA) of a water droplet on the surface of the untreated ETFE film and both the ETFE-SA membrane with a low and high degree of sulphonation (d.o.s.).

	ETFE (30 μm)	ETFE-SA (low d.o.s., upper surface)	ETFE-SA (low d.o.s., lower surface)	ETFE-SA (high d.o.s., upper surface)	ETFE-SA (high d.o.s., lower surface)
CA	94 °	85 °	101 °	61 °	66 °

The water contact angle (CA) measurement in Publication II is done for three different samples. The first is an untreated ETFE film, the second is an ETFE-SA membrane with a low degree of sulphonation and the third is an ETFE-SA membrane with a high degree of sulphonation. Both sides of the ETFE-SA membranes are investigated and the mean values of 20 contact angle measurements of a water droplet are presented in Table 6.1. The 'high d.o.s.' refers to the sulphonation level, which is adequately high for a good proton conductivity and efficiency in the DMFC and the 'low d.o.s.' to a substantially lower amount of sulphonic acid groups in the membrane. The 'upper surface' refers to the side of the membrane facing the incoming ion beam during the irradiation treatment and the 'lower surface' to the exit side of the ion beam. The error estimate for the contact angle (CA) values is $\pm 5\,^{\circ}$. Because the lower CA value refers to the lower surface hydrophobicity, there can be seen a large difference in surface hydrophobicities between the untreated ETFE film and the ETFE-SA membrane, which has a high degree of sulphonation. The CA values of both sides of ETFE-SA with a low degree of sulphonation are much higher compared to the corresponding values of ETFE-SA with a high degree of sulphonation.

The wetting and surface hydrophobicity properties of the Nafion® membrane have been investigated widely in many studies, e.g. [154,205–209]. Zawodzinski *et al.* [154]

measured contact angles on prehydrated Nafion® membranes and also as a function of drying time or water content of the membrane. They concluded that the contact angles of water are somewhat lower on the membrane of lower equivalent weight, the contact angles of water are about the same for membranes of different thickness, but the same equivalent weight, and the contact angles of water on the membranes became higher as the membranes dried out or water content decreased [154]. As a general observation, the surface of Nafion ® is clearly hydrophobic (CA > 90 °) [205–207]. Therefore in some studies, its surface hydrophobicity has been tried to decrease, e.g. with a low energy plasma treatment [209].

For the ETFE-SA membrane, the sulphonation is observed to decrease the contact angles and surface hydrophobicity, because of the presence of the hydrophilic sulphonic acid groups. Brack *et al.* [208] have made similar observations concerning styrene grafted and sulphonated ETFE and FEP membranes: sulphonation is observed to decrease the contact angles and increase surface energies of the membranes in comparison to those of the starting films and the grafted films. Because less pores and roughness are also seen in the AFM images taken from the irradiation side of ETFE-SA, it is supposed that the morphological differences might also affect the surface hydrophobicity. The contact angles are lower on the side facing the irradiation (upper surface).

The nature of irradiation method (deceleration of the ions within the membrane and subsequent changes both in stopping and dose profile) is most certainly affecting the concentration profile of the reactive sites for sulphonation. An additional effect is produced by the secondary electrons released both from the polymer and the backing material of the sample holder used during the irradiation. As the detailed analysis of all these parameters is complicated, it is only concluded that the lower surface of the membrane - i.e. the exit side of the ions - is subjected to a higher absorbed dose than the upper surface. However, whether this correlates with sulphonic acid concentration is unclear as the hydrophobicity depends on numerous other factors

like surface roughness, crosslinking density and swelling.

6.2 Structural Properties

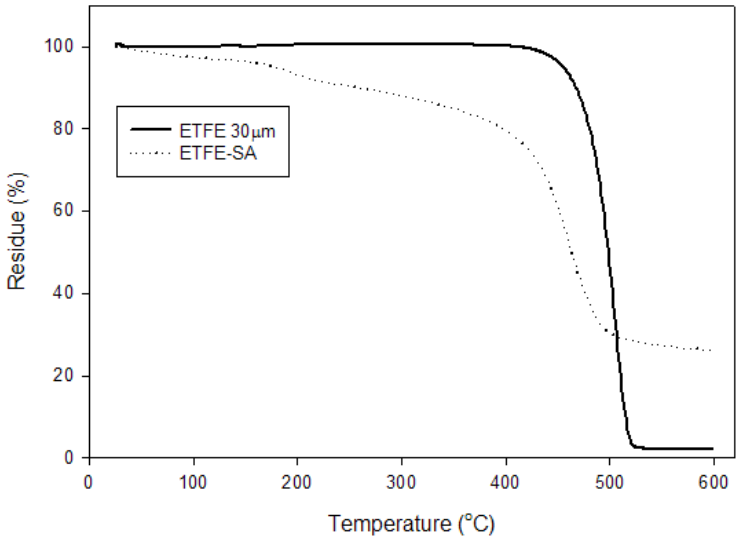

Figure 6.4: The thermostability curves for the ETFE film and the ETFE-SA membrane.

The initial ETFE polymer is typically semi-crystalline. For the pristine polymer film used in this study, a crystallinity of 34% is measured with wide angle X-ray scattering (WAXS). According to another study [133], the applied irradiation method is not detected to induce any significant changes in the overall crystallinity. It is known that of the different fluoropolymers, ETFE is exceptionally tolerant to ionizing radiation meaning that crosslinking is more favourable than chain scission. Consequently, after irradiation the film is crosslinked both by the crystallites and chemical crosslinks. Sulphonation, however, changes significantly the overall crystallinity. In case all the attached sulphonic acid groups and adsorbed water are located in the amorphous zone, they should reduce the overall crystallinity of the membrane to 22%. Yet, a value of 11% is detected with differential scanning calorimetry (DSC).

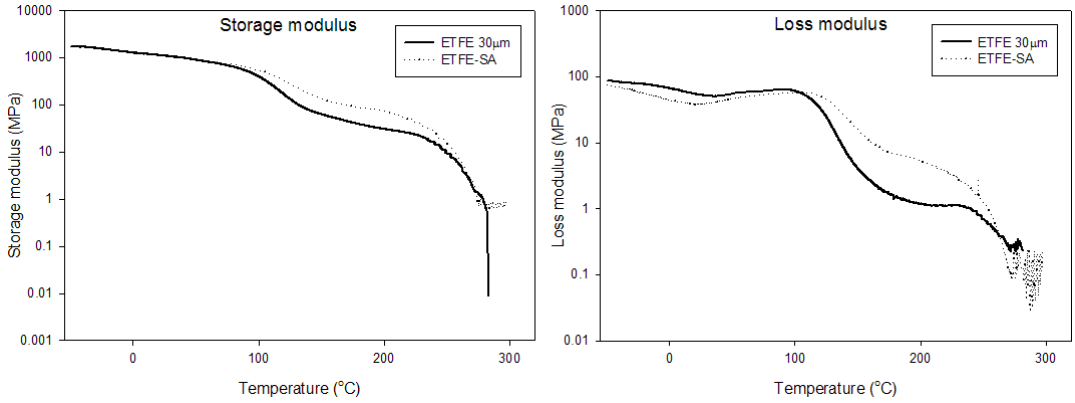

Figure 6.5: The storage and loss modulus for the ETFE film and the ETFE-SA membrane.

Because this measured crystallinity is only 50% of the calculated one, the sulphonation reaction has been concluded to induce crystal rupture. When comparing the amount of crosslinks and the swelling properties of the sulphonated ETFE with Nafion®, a clear difference is seen. This can be explained by structural differences. No chemical crosslinks are present in Nafion®, only the crystallites essentially limit its swelling. For Nafion® a crystallinity of 3-12% has been reported [105]. The ETFE-SA membrane has similar or higher crystallinity, but additionally, a significant amount of chemical crosslinks are formed both during the irradiation and the sulphonation, which highly restricts the swelling.

The thermostability curves (TGA curves) for the ETFE film and the ETFE-SA membrane are presented in Publication II and in Fig. 6.4 of this thesis. The untreated ETFE film shows a simple thermal degradation curve, where the degradation takes place in one step in the temperature range 415-525 °C. The mass loss of the ETFE-SA membrane occurs in several stages. One can see little change in weight of the sample in the temperature range 25-140 °C. This indicates most probably a loss of water bound to the sulphonic acid groups of the membrane. Approximately at 150 °C, a step-like change can be seen in the TGA curve followed by a more gradual loss of mass due to the loss of sulphonic acid groups in the material. Fi-

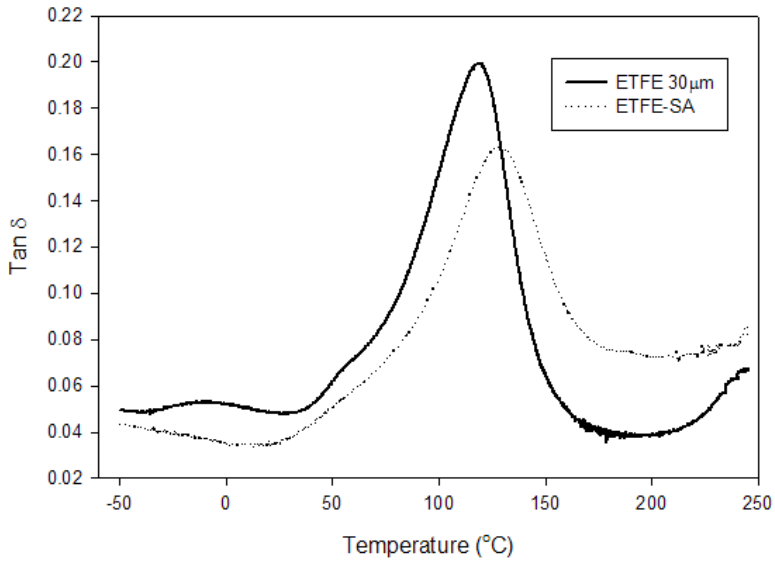

Figure 6.6: The T_g values for the ETFE film and the ETFE-SA membrane can be evaluated from the loss tangent curve.

nally, approximately in the temperature range 350-540 °C, thermal degradation of the polymer backbone occurs. The amount of residuals is high in the case of the ETFE-SA sample. This is probably due to the crosslinking of the ETFE material during the irradiation process.

The DMA curves for the ETFE film and the ETFE-SA membrane are presented in Publication II and in Fig. 6.5 of this thesis. In the temperature range -50 - 270 °C the samples show the behaviour of a solid material ($E' > E''$). Broad peaks can be seen in the tan δ curve for both samples (Fig. 6.6). The peak maximum corresponds to the glass transition temperature (T_g) for the samples. The T_g values for the untreated ETFE film and the ETFE-SA membrane are 119 °C and 128 °C, respectively.

The glass transition can also be seen in the storage modulus curve as a step-like transition and the loss modulus as a maximum of the curve. Sulphonic acid groups in the membrane cause a change in the glass transition temperature. After the glass

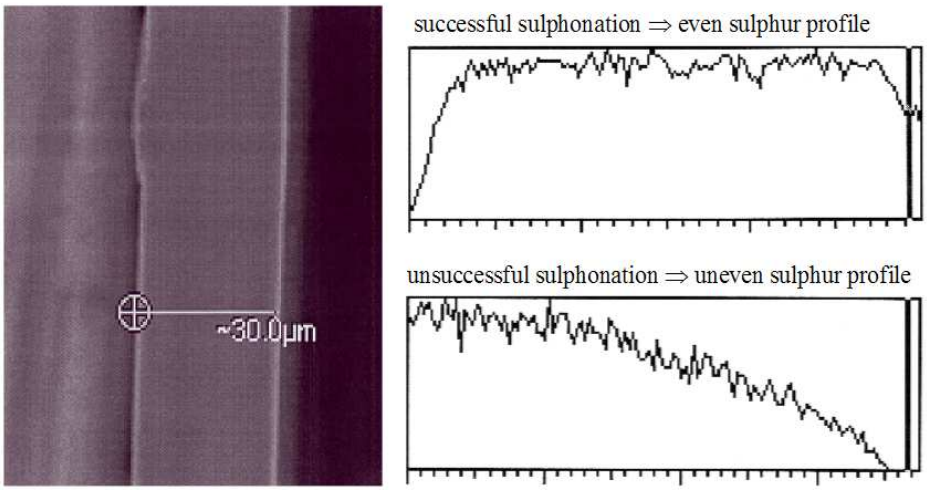

Figure 6.7: Inhomogeneous and homogeneous sulphur profiles along the cross-sections of two different ETFE-SA membranes are measured with the EDX.

transition region a clear difference between storage modulus values for the two materials can be seen. The loss modulus for ETFE-SA is clearly higher at the rubber plateau area, which is in a temperature range 170-230 °C. This can be an indication of crosslinking. The drop of storage modulus near 0.01 MPa at a temperature of 270 °C corresponds to melting of ETFE. In the case of the ETFE-SA membrane, the storage modulus drops only slightly at a temperature of 270 °C to approximately 1 MPa. This indicates that the material softens, but still stays in a solid state. This kind of behaviour is very characteristic for crosslinked polymers. A similar drop can be seen in the loss modulus curve at a temperature of 270 °C. The DMA measurements together with the TGA results show clearly that crosslinking takes place during the irradiation process of the ETFE-SA membrane.

Almeida *et al.* [210] have measured slightly lower glass transition temperatures for the Nafion® membrane compared to the value measured in this thesis for ETFE-SA. They measured T_g values for Nafion® 117 both in protonic and sodium form and observed two peaks in both cases. They concluded that the high-temperature peak (T_g = 230 °C) is assigned to the melting of crystalline domains and the low-

temperature peak (T_g = 120 °C) is attributed to the membrane transition into ionic clusters [210]. According to also other studies [211,212], the (lower) T_g value for the Nafion® membrane is around 110-120 °C.

The T_g value of the initial PVDF film is -40 °C, but according to the measurements of Hietala *et al.* [134], the T_g value of the PVDF-*g*-PSSA membrane cannot be detected. The shape of the bimodal melting endotherm changes, when the membrane is reheated so that the area under the lower melting peak increased and the area under the higher melting peak decreases [134]. A very weak transition is observed around 100 °C, which can be attributed to the glass transition of polystyrene, but as a most probable rationale, the grafting takes place in the entire amorphous region of the PVDF-*g*-PSSA and so also in the areas very close to the crystallite surfaces of the lamellae [134]. For the sPSO2 membrane Schuster *et al.* [143] measured that neither glass transition nor melting takes place below 300 °C.

During the manufacturing of ETFE-SA, the sulphonation reaction begins from the surface and continues towards the center of the membrane. An example of a successful and an unsuccessful sulphonation processes is presented in Publication II and in Fig. 6.7 of this thesis. Those sulphur profiles are measured with the EDX along the cross-sections of two different ETFE-SA membranes. The uneven sulphur profile shows that the degree of sulphonation (*d.o.s.*) is heterogeneous. In contrast, when an even plateau can be seen (covering approximately 85% of the length scale), it can be concluded that also sulphonation across the membrane is homogeneous.

The low concentration levels, which can be seen in the Fig. 6.7 near the surfaces are due to instrumental reasons, i.e. the position of the X-ray detector is slightly aside from the sample (not directly above) and thus the registered X-ray counts coming from the sample are not completely reliable. This can also be evidenced by analyzing the relative concentrations as a point analysis both at different points of the cross-section as well as at the surface. The homogeneous sulphur profile will

lead to good proton conductivity and high performance in the fuel cell, which can also be verified with the conductivity measurements and the DMFC tests.

6.3 MeOH Permeability

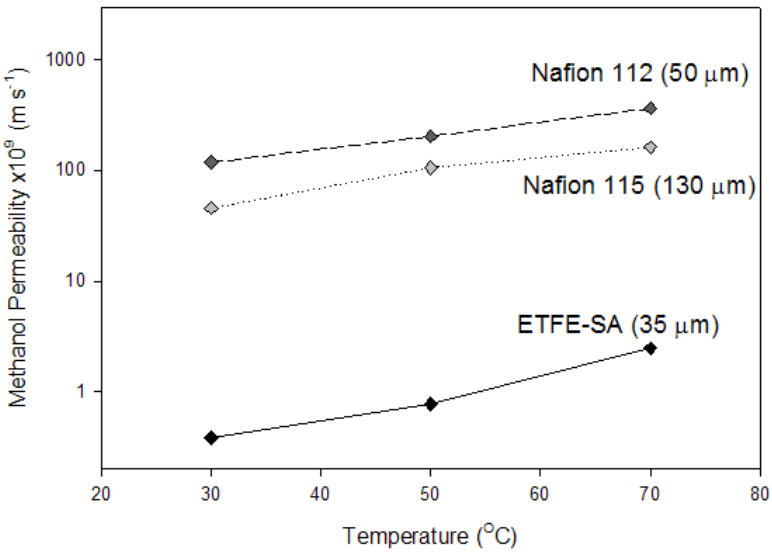

Figure 6.8: Effect of the temperature on the methanol permeability P through ETFE-SA, Nafion® 112 and Nafion® 115 measured using the diffusion cell.

The MeOH permeability values measured with the diffusion cell (and calculated according to Eq. 5.4) are presented in Publication II and in Fig. 6.8 of this thesis. The measured MeOH permeability values for the Nafion® membranes are of the same magnitude as can be found from the literature [138, 184], whereas the values for ETFE-SA are less than 0.8% of the corresponding values for Nafion® 112 and less than 1.5%, when compared to Nafion® 115. It can also be seen that when the temperature is raised from 30 to 70 °C, the MeOH permeability through the ETFE-SA membrane increases to about seven times higher value.

Quite similar results, as with the diffusion cell, are obtained when the MeOH crossover is measured under real DMFC conditions according to the method intro-

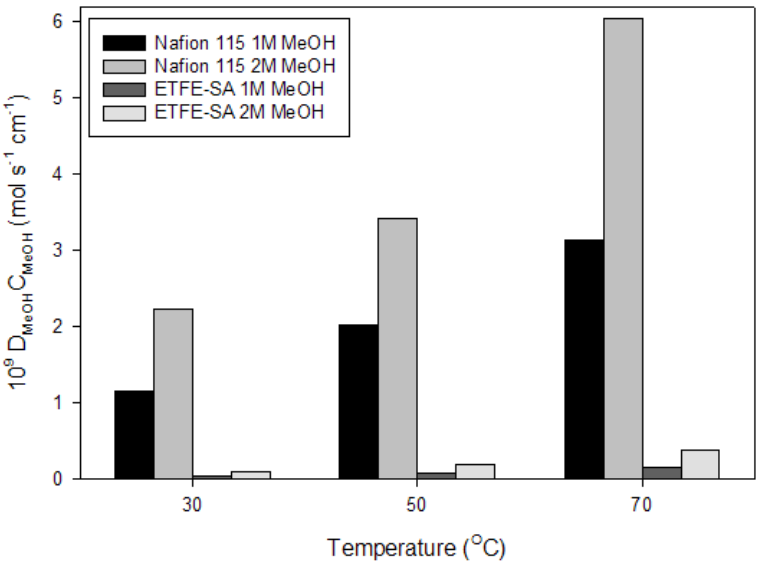

Figure 6.9: Methanol permeability ($D_{\mathrm{MeOH}}c_{\mathrm{MeOH}}$) through the Nafion® 115 and the ETFE-SA membranes as a function of temperature measured under true DMFC conditions.

duced by Ren *et al.* [89]. The MeOH permeability ($D_{\mathrm{MeOH}}c_{\mathrm{MeOH}}$), measured under true fuel cell conditions with 1 and 2 M MeOH solutions, through the investigated membranes as a function of temperature is presented in Publication I and in Fig. 6.9 of this thesis. It can be seen that the MeOH permeability through ETFE-SA is very low: The calculated D_{MeOH} and $D_{\mathrm{MeOH}}c_{\mathrm{MeOH}}$ values (Eqs. 5.5 and 5.7) are 90% lower for the ETFE-SA membrane than for the Nafion® 115 membrane.

As a comparison, Kallio *et al.* [138] have measured MeOH diffusion coefficients in the PVDF-*g*-PSSA membrane and concluded that they are about 30% of the corresponding values of Nafion® 115 in a temperature range 30 - 70 °C. Altogether, the low MeOH permeability is a very important property for membranes, which are planned to be used in the DMFC. Thus, because of very low MeOH permeability, the ETFE-SA membrane has proved to be promising candidate for the DMFC.

6.4 Swelling and Fractionalization

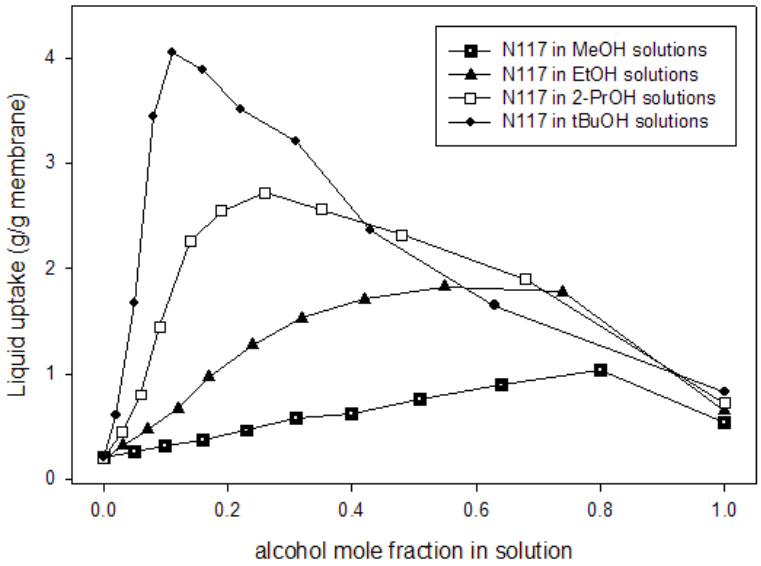

Figure 6.10: Solvent uptake of Nafion® 117 membrane in different alcohol-water mixtures after equilibration for 3-7 days at room temperature.

The total liquid uptakes of Nafion® 117 in different alcohol-water mixtures are presented in Publication III and in Fig. 6.10. The liquid uptake is lowest in MeOH-water mixtures and increases considerably, when alcohols of higher molecular mass are used - especially in *t*BuOH-water mixtures, a huge swelling is observed. This is quite as expected, because the Nafion® membranes are not chemically crosslinked and are known to be soluble in alcohol solutions, e.g. Nafion® 117 has been shown to dissolve gradually in MeOH-water mixtures [213]. For Nafion® 117, the maximum solvent uptake is observed for MeOH, EtOH, 2-PrOH and *t*BuOH mole fractions of 0.8, 0.55, 0.25 and 0.15, respectively.

A qualitatively different behaviour is observed for the swelling of PVDF-*g*-PSSA and ETFE-SA (Fig. 6.11). For PVDF-*g*-PSSA, the maximum solvent uptake is measured for pure water and solvent uptake decreases towards higher alcohol mole

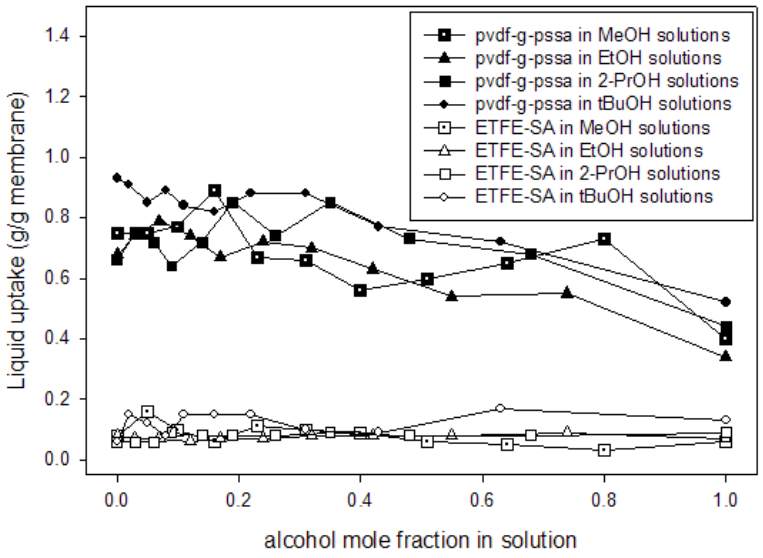

Figure 6.11: Solvent uptake of PVDF-*g*-PSSA and ETFE-SA membranes in different alcohol-water mixtures.

fractions. The liquid uptake results for Nafion® 117 and PVDF-*g*-PSSA in MeOH-water mixtures are consistent with previously published data [132]. If compared to Nafion® 117, the swelling of ETFE-SA and PVDF-*g*-PSSA is much lower and virtually independent of the kind of alcohol. This is particularly true for ETFE-SA, for which the solvent uptake is very low (less than 15 w-% over the whole concentration range). The very low swelling and dimensional changes of the ETFE-SA membrane - also when using high MeOH concentrations, is a positive phenomenon from the point of view of the DMFC application. This also provides a rational for the measured very low MeOH permeability through the ETFE-SA membrane.

The different swelling behaviour directly reflects the different mechanical properties of the investigated membranes. Provided that osmosis is the major swelling process, the low solvent uptake of ETFE-SA and PVDF-*g*-PSSA suggests high elastic constants for these two types of membrane. In contrast to Nafion® 117, the polymer backbones of ETFE-SA and PVDF-*g*-PSSA are significantly stiffer. This

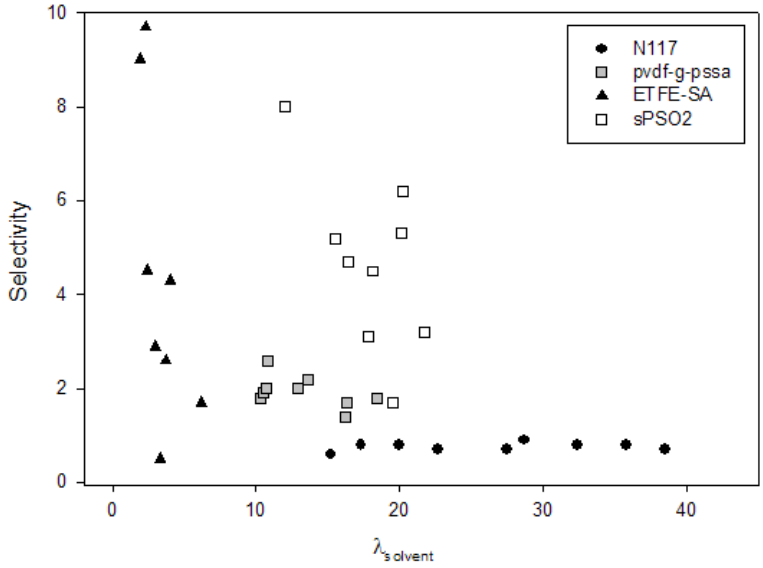

Figure 6.12: Selectivity for water uptake from water-MeOH mixtures as a function of λ_{solvent} (number of solvent molecules per sulphonic acid group).

leads to higher internal pressures compensating for the osmotic swelling pressure at lower degrees of swelling. That is particularly true for ETFE-SA, in which the -SO_3 groups are directly connected to the ETFE-backbone and which shows extremely low swelling. The structure of hydrophilic (proton conducting) channels through ETFE-SA differs from the one inside the Nafion® membranes. This phenomenon is closely connected to the lower amount of water molecules vs. sulphonic acid groups inside the ETFE-SA membrane and lower conductivity.

The water selectivity (as defined by Eq. 5.3) of solvent uptake in MeOH-water mixtures is plotted as a function of λ_{solvent} (number of solvent molecules / number of -SO_3 groups in membrane) in Fig. 6.12. For Nafion® 117 the data do not give significant indication for preferential solvent uptake, i.e. the alcohol mole fractions in the membrane and in the liquid are almost identical, which is consistent with the results of earlier reports [87, 89, 213]. For membranes with lower swelling (PVDF-*g*-PSSA, ETFE-SA and sPSO2) however, preferential water uptake is observed for all

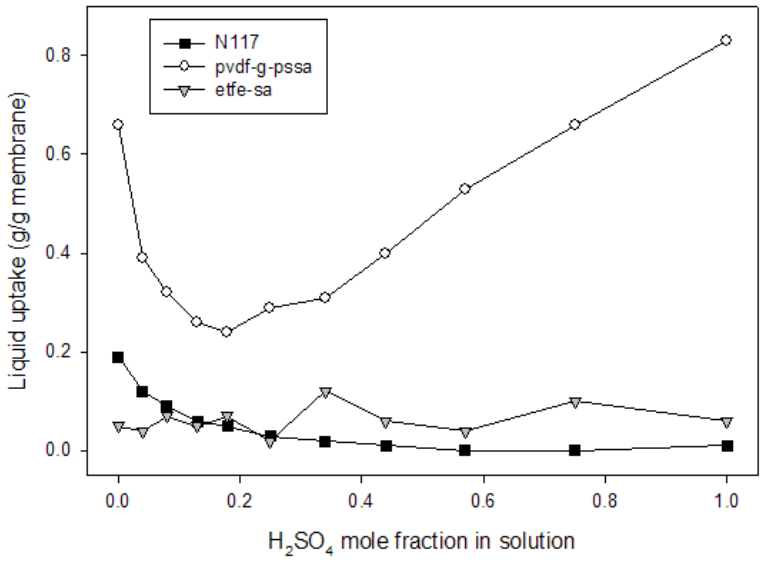

Figure 6.13: Total uptake of aqueous sulfuric acid mixtures of different concentration.

kinds of alcohols.

Clear trends can be observed for the selectivity: preferential water uptake (alcohol rejection) correlates with high ion exchange capacity (IEC) and low solvent uptake (swelling) indicating a preferred interaction of the ionic groups (-SO_3^-, H^+) and the groups on the backbone carrying partial charges (e.g. sulphone units (-SO_2-) in the sPSO2) with water. The alcohol may then be restricted to the central bulky part of the solvated hydrophilic domain as indicated by a water and EtOH diffusion study on swollen highly sulphonated polyethylene by Freger *et al.* [214]. Although the MeOH diffusion coefficients are found to be significantly lower than the water diffusion coefficients in these membranes, their temperature dependency, i.e. the activation enthalpies, are virtually identical. With decreasing swelling, i.e. with successive decrease of "bulky" solvent within the hydrophilic channels and pores, an increasing rejection of alcohol is then anticipated.

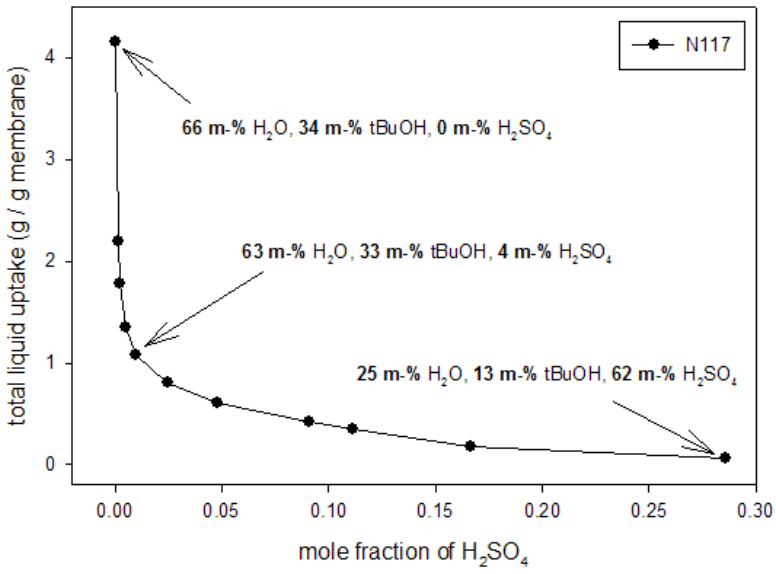

Figure 6.14: Effect of the H_2SO_4 increment on the swelling of the Nafion® 117 membrane in *t*BuOH-water mixtures.

The total liquid uptake of Nafion® 117, PVDF-*g*-PSSA and ETFE-SA in different H_2SO_4-water mixtures is presented in Publication III and in Fig. 6.13 of this thesis. Especially for Nafion® 117 the uptake of solution is decreasing with increasing H_2SO_4 concentration, which is clearly indicating that the osmosis is a major driving force in the swelling process. For ETFE-SA, the swelling is almost unaffected by the H_2SO_4 concentration which is in favour of a kind of "free volume" of a rigid structure, which is filled with liquid. For PVDF-*g*-PSSA, a minimum is observed in the swelling and the increasing swelling with increasing H_2SO_4 concentrations and time is probably the result of a proceeding sulphonation reaction under these conditions. The effect of H_2SO_4 on the swelling of Nafion® 117 in alcohol-water mixtures is also tested and an example of that is presented in Fig. 6.14. A mass ratio of 2 / 1 is chosen for water and *t*BuOH corresponding to the mixture, for which a very high total swelling is observed (see Fig. 6.10). As a result, a drastic decrease in swelling is already observed at very low H_2SO_4 concentrations again supporting that osmosis is the major driving force in the swelling process.

6.5 Performance in the DMFC

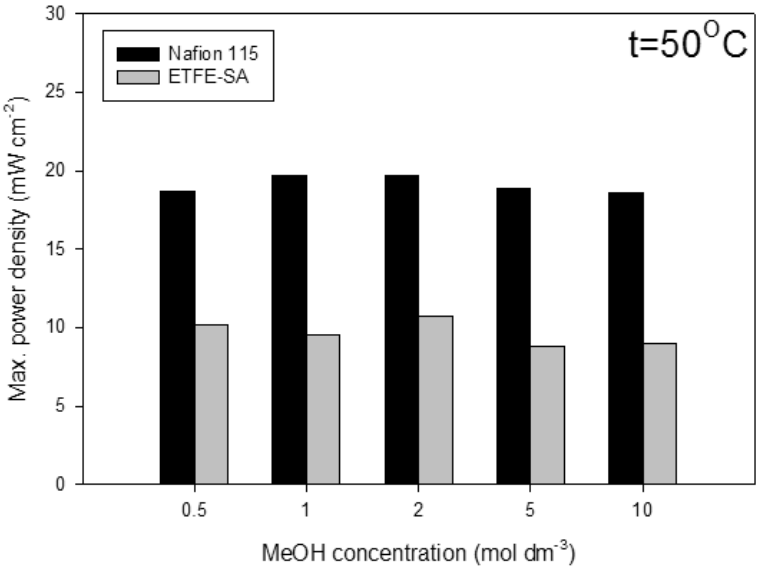

Figure 6.15: The maximum power densities as a function of MeOH concentration for the Nafion® 115 and the ETFE-SA membranes at 50°C.

The measured maximum power densities for the Nafion® 115 and the ETFE-SA membranes as a function of MeOH concentration and temperature are presented in Publication I of this thesis. In Fig. 6.15, where measured maximum power densities at 50°C are presented, it can be seen that measured maximum power densities for ETFE-SA are about the half of corresponding values for Nafion® 115 over the whole concentration range. The conductivity of the ETFE-SA membrane is much lower compared to the other investigated membranes (see Table 4.1), but the area resistance is quite the same as for the Nafion® 115 membrane. Because the ETFE-SA membrane is very thin and the MeOH permeability through the membrane is very low, the DMFC performance of ETFE-SA is higher than one might expect just by comparing the conductivities. However, in a temperature range 30-70 °C, the performance of the ETFE-SA membrane is 40-65% lower compared to Nafion® 115. If the cathode gas is changed from oxygen to air, the efficiency decreases 10-40% depending on the temperature. The relative changes are observed to be almost equal

for both of the investigated membranes.

When the DMFC is operated with the Nafion® 115 membrane and the cathode gas (oxygen/air) is humidified, no significant changes are observed in the cell performance compared to the operation with dry gas (RH = 0%). With saturated oxygen (RH = 100%), only 0-5% decrease in the cell performance is observed and that small change is proposed to result from blocking effects of extra H_2O molecules in the cathode flow channels (cathode flooding). When using the ETFE-SA membrane, the cathode gas humidification is observed to improve the cell performance. Depending on the temperature and cathode gas (oxygen/air), the improvements in the measured power densities are 10-200%. The minimum improvements (10-25%) are observed with oxygen cathode at 30 °C and the highest improvements with air cathode at 70 °C (180-200%). Performance improvements for all the examined MeOH concentrations (0.5-10 M) are of the same magnitude. Because the thickness of the ETFE-SA membrane is only 35 μm and its water uptake is very low (Table 4.1), the performance loss caused by the dry cathode gas (RH = 0%) is observed to increase as a function of temperature. It is presumable that poor performance with the dry cathode gas is a consequence of local drying of the membrane, which affects the membrane conductivity.

When using dry cathode gas and 1 bar (g) back pressure both for the cathode and the anode side, the power densities are observed to increase 1-20% (Nafion® 115) and 10-270% (ETFE-SA) compared to the power densities with small back pressures (cathode: 0.2 bar (g), anode: 0 bar (g)). For both the membranes, the improvements increase as a function of temperature and MeOH concentration. At low MeOH concentrations (0.5 - 2 M) the performance improvements for the Nafion® 115 membrane are only 1-10%. For the Nafion® 115 they result mainly from the accelerated reaction kinetics, especially on the cathode side. For ETFE-SA the improvements are of the same magnitude or even higher than when humidified cathode gas is used. Because of low values for MeOH permeability (Figs. 6.8 and 6.9), it is

suggested that low performance of ETFE-SA (especially at 70 °C with dry cathode gas) results from the lack of water molecules inside the membrane, which decreases conductivity. In addition, the performance of the ETFE-SA membrane is observed not to increase more, if both the cathode side humidification and the 1 bar (g) back pressures are used.

In the DMFC tests, the ETFE-SA membrane was observed to be mechanically and chemically stable. The longest continuous test with the ETFE-SA membrane lasted more than 2000 h and no decrease in the performance was observed during that period. During that time the cell temperature was at 30-85 °C and the efficiency tests were done with different operational parameters (temperature, gas relative humidity, etc.). During that long-term stability test, the cell temperature was about 1300 h at 30 °C, 400 h at 50 °C and 300 h at 70-85 °C. Some of the best performance values were measured during the last test week of the total 2000 h test. The ETFE-SA membrane was finally observed to break, when the cell temperature was increased higher than 100 °C.

Because the electrode structures have only been optimized for Nafion®, both the contacts within the MEA and their stabilities are supposed to be non-optimal for the ETFE-SA membrane. Consequently, lower performance values than expected on the basis of area resistance for ETFE-SA in the DMFC tests are recorded. Another important parameter defining the stability and resistive losses of the MEA is the mutual compatibility of polymers used both as the membrane and as the binder and proton conductor in the electrodes. In the case, where ETFE-SA is tested with Nafion® containing electrodes this requirement is not fulfilled. A poor bonding of the catalyst layers to the grafted membranes has also been reported in some other studies [215, 216]. Therefore, the lower efficiency of ETFE-SA is probable resulting from the lower conductivity and high ohmic losses of the MEAs (a high contact resistance between the membrane and the electrodes).

6.6 Current Distribution in the Free-Breathing DMFC

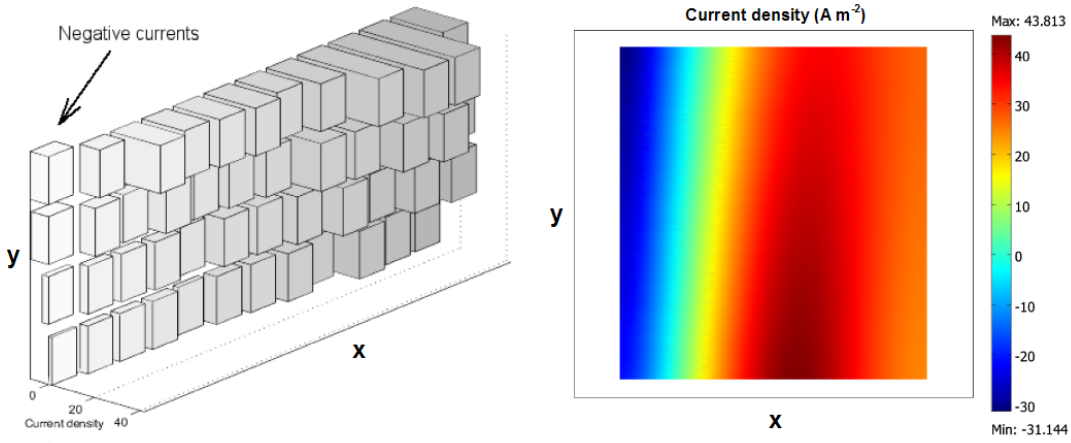

Figure 6.16: The measured (left) and modelled (right) current density distribution at 70 °C (3 M MeOH, flow rate 3.3 $\times 10^{-9}$ m^3 s^{-1}, E_{cell} = 0.5 V).

Because the areal variations in the cell current give indirect information of local concentrations of the reacting species and other mass transfer phenomena, the complicated connections between different operation parameters can be clarified. It can be immediately seen during the fuel cell testing, in which part of the electrode most of the current is produced and how even is the current distribution. Additionally, it can be seen how the current distribution changes along the MeOH flow channel and how much the MeOH crossover phenomenon decreases the cell performance locally. Generally, the best performance values are measured, when the current density distribution is even and the deviations from that even current density distribution are observed to increase as a function of MeOH concentration. Especially at low cell voltages, mass transport to the cathode is observed to be dominating loss mechanism and that can be seen during the current distribution measurements as a steep decrease in current densities in a vertical direction: most of the current is produced at the twelve lowest cathode segments (see figures of Publication IV).

It is also observed at higher current densities and especially at lower tempera-

tures that the air (oxygen) convection towards the cathode is inadequate in a free-breathing DMFC. Because the power production of the free-breathing DMFC is proportional to the oxygen concentration at the cathode side, inadequate air convection leads to uneven current distribution. As a consequence, when the cell is operated with a high current, almost all of the current is produced at the twelve lowest cathode segments. The air convection is inadequate towards the higher segments and very low current density values are measured, especially from the segments near the upper edge. The performance of the DMFC is known to be affected a lot by the cell temperature [124, 217]. According to the current distribution measurements of the free-breathing DMFC, an increase in temperature is observed to both enhance the cell performance and smooth the current distribution, which can be explained mainly as an increased air convection and decreased activation overpotentials at the electrodes.

Although the proton conductivities of Nafion® 117 and PVDF-*g*-PSSA are similar, the measured maximum power densities of PVDF-*g*-PSSA are 20-50% lower than the corresponding values of Nafion® 117. Because the open circuit voltage and maximum performance values of PVDF-*g*-PSSA and Nafion® 117 at low MeOH concentrations (0.5 - 3 M) are more similar than at higher concentrations (5 - 10 M), the MeOH crossover rate through the PVDF-*g*-PSSA membrane is probably higher than through the Nafion® 117 membrane. There are also other structural differences between the membranes and it is presumable that the contact between the electrodes and the PVDF-*g*-PSSA membrane is not as good as with Nafion® 117.

The highest power densities for Nafion® 117 and PVDF-*g*-PSSA are measured with a 1 M MeOH solution at all cell temperatures used (30, 50 and 70 °C). The observation concerning Nafion® 117 is similar to what has been reported in other studies [122, 124]. When the MeOH concentration is increased to 3 M or higher, the cell performance decreased and that is seen as a more uneven current distribution.

The performance decrease with higher MeOH concentrations is mainly caused by the MeOH crossover phenomenon, which lowers the cell voltage and with the segmented DMFC this can also be observed as a change in the shape of the current distribution. The lowest adequate MeOH stoichiometry, for which the performance of the DMFC is no longer MeOH mass transfer limited, is also measured at different temperatures. In most cases, a MeOH flow rate of 17×10^{-9} m^3 s^{-1} (1 ml min^{-1}) is high enough to give good performance values. Increasing the stoichiometry above 5 is useful only, when the DMFC is operated at very high current densities.

During the current distribution measurements, the DMFC with a segmented cathode is found to be a very convenient tool for investigation of areal relations between the MeOH concentration and the flow rate. As an example, when the MeOH concentration is 3 M and the MeOH flow rate of 3.3×10^{-9} m^3 s^{-1} (0.2 ml min^{-1}), which corresponds to the total stoichiometry of 7, the current densities increase along the MeOH flow channel and the highest current densities are located at the very end of the MeOH flow channel. This can be explained with the decrease of MeOH concentration. The electrochemical oxidation of MeOH takes place and due to the low MeOH flow rate, the MeOH solution dilutes and its concentration approaches the optimum value towards the end of the flow channel. Resulting from the decreased MeOH concentration, also the MeOH crossover rate is lower at the end of the flow channel. More detailed analysis concerning effects of different operation parameters on current distribution are presented in Publication IV.

The developed 3D model for the free-breathing DMFC is described in detail in Publication V. In this developed model, the *Navier-Stokes equation* is used for modelling Newtonian flow of MeOH and water in the anode flow field and also free convection of air in the cathode flow field. The *Stefan-Maxwell equation* is used for modelling multicomponent diffusion of gaseous species in the porous cathode transport layer (PTL) and *Brinkman's equation* for modelling the flow of MeOH and water in the anode PTL. The *Tafel equation* is used to describe electrochemical reactions at the

cathode and the linearized *Butler-Volmer equation* at the anode. The MeOH flow in the membrane (MeOH crossover) is described with *Fick's law* of diffusion and drag of protonic current. The only fitted parameter in the model is the parameter ψ for the MeOH oxidation rate at the cathode. ψ is fitted according to the measured current distributions of Publication IV.

During the experimental measurements, it is observed that the current densities can vary significantly inside the DMFC and in some cases even negative currents are measured. This can happen, when the MeOH crossover is relatively high and the cell is operated with relatively low current densities. An example of measured local negative currents is presented in Publication IV and at the left in Fig. 6.16 of this thesis. The cell voltage is 0.5 V and the flow rate of 3 M MeOH is 3.3×10^{-9} m^3 s^{-1} (0.2 ml min^{-1}). The current densities are negative near the MeOH inlet, because the DMFC is operated with relatively low current density and the MeOH crossover is dominating at those cathode segments. The corresponding modelled current density distribution ($\psi = 1.15 \times 10^{-9}$ m s^{-1}) is presented at the right in Fig. 6.16 and it is quite similar to the measured one. The model predicts that the current production of the DMFC can be locally negative, when the MeOH crossover rate is high near the MeOH inlet. The current densities increase along the MeOH flow direction (x-axis), which can be explained with a decrease of the MeOH concentration at the anode. The MeOH concentration decreases due to the electrochemical reactions and as a result, the effect of MeOH crossover is reduced and the current production again turns positive. More calculated current distributions and concentration profiles of the reactants are presented in in Publication V.

Altogether, the current distribution is observed to be closely connected to the local concentrations and mass flows of the reacting species. The local power production is observed to be proportional to the local oxygen concentration at the cathode side. As a consequence, inadequate air convection together with the MeOH crossover phenomenon decreases the cell performance. At high MeOH concentrations, the MeOH

crossover and the mass transfer of air are the main limiting factors of the cell performance, especially at low and high current densities, respectively. The developed model is in reasonable agreement with both the measured current distributions and polarization curves. The spatial information gained of mass transfer phenomena inside the DMFC is valuable for the optimization of the DMFC operation parameters.

7 Summary and Concluding Remarks

In this thesis, the properties of four different kind of membranes for the direct methanol fuel cell (DMFC) are investigated using various experimental techniques and this work can be seen as a part of the DMFC development work towards true commercial applications. The benefits of extensive membrane characterization are demonstrated, especially in the studies concerning the ETFE-SA membrane. During the experimental work, many remarkable structural differences between different membranes are observed e.g. the connections between the surface properties of ETFE-SA and its manufacturing process are clarified.

The clear variations in swelling behaviour of the investigated membranes are explained in this thesis in terms of mechanical properties, concentration of ions and polarity of the polymer backbone. The huge swelling of Nafion® in water - alcohol solutions is explained by penetration of alcohol molecules into the hydrophilic regions to form ionic cluster regions together with water and sulphonic acid groups. Preferential water uptake (alcohol rejection) is observed to correlate with a high ion exchange capacity and a low swelling, indicating a preferential interaction of the ionic groups ($-SO_3^-$, H^+) with water. A high MeOH rejection is only observed for membranes with low swelling and the total swelling is observed to decrease significantly in the presence of H_2SO_4, indicating that osmosis is a major driving force in the swelling process.

The most attractive aspects concerning the new ETFE-SA membranes are their low price and very low MeOH permeability (less than 2%) compared to the commercial Nafion® membranes. On the basis of this thesis, the durability of ETFE-SA is observed to be sufficient for DMFC applications at low temperatures ($T < 80$ °C), as over 2 000 h DMFC testing was carried out without any loss of performance. The investigations concerning the PVDF-*g*-PSSA membrane have mainly confirmed some previous results and showed that its swelling is notably lower compared to

the Nafion® membranes. Also, some material properties of the sPSO2 membrane are observed to be very promising, but the main challenges of this membrane are still related to its mechanical properties and compatibility with the electrodes. Altogether, the properties of investigated membranes are observed to vary in a wide range and their performance values in the DMFC are still lower compared to the commercial Nafion® membranes. However, on the grounds of the experiences and results achieved in this thesis the investigated membranes are considered to be worth of further study. Also, the characterization methods described in this thesis can be applied to the investigations of other types of polymer membranes.

The free-breathing DMFC with a segmented cathode current collector is used in this thesis to achieve better understanding of the occurring mass transfer phenomena and to clarify complicated connections between different operation parameters. As a result, the current distribution is observed to be closely connected to the local concentrations and mass flows of the reacting species, especially the local power production is observed to be proportional to the local oxygen concentration at the cathode. At high MeOH concentrations (5-10 M), the MeOH crossover and the mass transport of air are the main limiting factors of the cell performance, especially at low and high current densities, respectively.

A three-dimensional model is developed for a free-breathing DMFC. The MeOH crossover and other mass transfer phenomena are investigated computationally and the model validations are done using the current distribution measurements. The developed model describes current production and mass transfer phenomena in a free-breathing DMFC, when different operation parameters are varied on a large scale. The model also describes with reasonable accuracy the existence of the measured electrolytic domains, i.e. the regions of negative current densities. As a future work, the model is suggested to be developed further by describing the electrodes and electrode reactions more profoundly and doing the model validations both with the polarization curves and the current distribution measurements.

References

[1] A. Appleby, F. Foulkes, *Fuel Cell Handbook*, Van Nostrand Reinhold, New York, 1989.

[2] EG&G Technical Services, Inc. Science Applications International Corporation, *Fuel Cell Handbook*, 6th Edition, U.S. Department of Energy, National Energy Technology Laboratory, 2002.

[3] K. Kordesch, G. Simader, *Fuel Cells and Their Applications*, Wiley-VCH, 1996.

[4] W. Grubb, *Proceedings of the 11th Annual Battery Research and Development Conference*, PSC Publications Committee, Red Bank, NJ, 1957, p. 5.

[5] W. Grubb, US Patent 2,913,511 (1959).

[6] W. Grubb, L. Niedrach, *J. Electrochem. Soc.* **107** (1960) 131–135.

[7] R. Souzy, B. Amerudi, *Prog. Polym. Sci.* **30** (2005) 644–687.

[8] M. Perry, T. Fuller, *J. Electrochem. Soc.* **149** (2002) S59–S67.

[9] H. Gibbs, V. Vienna, R. Griffin, US Patent 3,041,317 (E.I. DuPont de Nemours and Company) (1962).

[10] L. Niedrach, H. Alford, *J. Electrochem. Soc.* **112** (1965) 117–124.

[11] L. Niedrach, Elecrode structure and fuel cell incorporating the same, US Patent 3,297,484 (1967).

[12] M. Wilson, Membrane catalyst layer for fuel cells, US Patent 5,211,984 (1993).

[13] M. Wilson, S. Gottesfeld, *J. Appl. Electrochem.* **22** (1992) 1–7.

[14] M. Wilson, J. Valerio, S. Gottesfeld, *Electrochim. Acta* **40** (1995) 355–363.

[15] V. Mehta, J. Cooper, *J. Power Sources* **144** (2003) 32–53.

[16] Johnsson-Matthey, *ETSU Direct Methanol Fuel Cell Review*, Tech. rep., UK Department of Trade & Industry (February 1995).

[17] Jülich unveils DMFC-powered JuMOVe vehicle, Fuel Cells Bulletin Vol. 2004 Issue 12 p.3-4.

[18] P. Fontela, A. Soria, J. Mielgo, J. Sierra, J. Blas, L. Gauchia, J. Martinez, *J. Power Sources* **169** (2007) 184–193.

[19] MTI Micro deals with military OEM, satcoms, Fuel Cells Bulletin Vol. 2006 Issue 3 p.2-3.

[20] SFC delivers portable military fuel cell systems, Fuel Cells Bulletin Vol. 2007 Issue 1 p.7-8.

[21] W. Knight, Fuel cell propelled aircraft prepairing to fly, New Scientist (May 2003).

[22] Flight tests on way for Boeing fuel cell airplane, Fuel Cells Bulletin Vol. 2007 Issue 5 p.2-3.

[23] G. Sattler, *J. Power Sources* **86** (2000) 61–67.

[24] S. Kamarudin, W. Daud, S. Ho, U. Hasran, *J. Power Sources* **163** (2007) 743–754.

[25] C. Lamy, J.-M. Léger, S. Srinivasan, *Direct Methanol Fuel Cells: From a Twentieth Century Electrochemist's Dream to a Twenty-First Century Emerging Technology*, in: J. Bockris, B. Conway, R. White (Eds.), *Modern Aspects of Electrochemistry*, Vol. 34, Kluwer Academic/Plenum Publishers, New York, 2001.

[26] X. Ren, P. Zelenay, S. Thomas, J. Davey, S. Gottesfeld, *J. Power Sources* **86** (2000) 111–116.

[27] K. Tüber, M. Zobel, H. Schmidt, C. Hebling, *J. Power Sources* **122** (2002) 1–8.

[28] F. Urbani, G. Squadrito, O. Barbera, G. Giacoppo, E. Passalacqua, O. Zerbinati, *J. Power Sources* **169** (2007) 334–337.

[29] W. Qian, D. P. Wilkinson, J. Shen, H. Wang, J. Zhang, *J. Power Sources* **154** (2006) 202–213.

[30] C. Chen, D. Liu, C. Huang, C. Chang, *J. Power Sources* **167** (2007) 442–449.

[31] IBM, Sanyo demo DMFC prototype for ThinkPad PC, Fuel Cells Bulletin Vol. 2005 Issue 5 p.1.

[32] Toshiba, Hitachi DMFCs feature in prototype audio players, cell phones, Fuel Cells Bulletin Vol. 2005 Issue 11 p.8.

[33] A. Heinzel, V. Barrágan, *J. Power Sources* **84** (1999) 70–74.

[34] K. D. Kreuer, *J. Membr. Sci* **185** (2001) 29–39.

[35] K. D. Kreuer, *Chem. Mater.* **8** (1996) 610–641.

[36] L. Gubler, S. Gürsel, G. Scherer, *Fuel Cells* **5** (2005) 317–335.

[37] N. Deluca, Y. Elabd, *J. Polym. Sci Part B: Polym. Phys.* **44** (2006) 2201–2225.

[38] M. Hickner, H. Ghassemi, Y. Kim, B. Einsla, J. McGrath, *Chem. Rev.* **104** (2004) 4587–4612.

[39] V. Neburchilov, J. Martin, H. Wang, J. Zhang, *J. Power Sources* **169** (2007) 221–238.

[40] M. Rikukawa, K. Sanui, *Prog. Polym. Sci.* **25** (2000) 1463–1502.

[41] N. Asano, K. Miyatake, M. Watanabe, *Chem. Mat.* **16** (2004) 2841–2843.

[42] L. Jörissen, V. Gogel, J. Kerres, J. Garche, *J. Power Sources* **105** (2002) 267–273.

[43] B. Bahar, A. Hobson, J. K. D. Zuckerbrod, Ultra-thin integral composite membrane, US Patent 5,547,551 (W.L. Gore) (1996).

[44] W. Liu, K. Ruth, G. Rusch, *J. New Materials for Electrochem. Systems* **4** (2001) 227–231.

[45] M. Janssen, J. Moolhuysen, *Electrochim. Acta* **21** (1976) 861–868.

[46] B. Beden, F. Kadirgan, C. Lamy, J. Leger, *J. Electroanal. Chem.* **127** (1981) 75–85.

[47] G. Troughton, A. Hamnett, *Bull. Electrochem.* **7** (1991) 488–492.

[48] J. Wang, H. Nakajima, H. Kita, *J. Electroanal. Chem.* **250** (1988) 213–217.

[49] W. Lizcano-Valbuena, V. Paganin, C. Leite, F. Galembeck, E. Gonzeles, *Electrochim. Acta* **48** (2003) 3869–3878.

[50] S. Gottesfeld, M. Wilson, *J. Electrochem. Soc.* **139** (1992) L28–L30.

[51] P. Fedkiw, W. Her, *J. Electrochem. Soc.* **136** (1989) 899–900.

[52] E. Taylor, E. Anderson, N. Vilambi, *J. Electrochem. Soc.* **139** (1992) L45–L46.

[53] T. Ralph, G. Hards, J. Keating, S. Champbell, D. Wilkinson, M. Davis, J. St-Pierre, M. Johnson, *J. Electrochem. Soc.* **144** (1997) 3845–3857.

[54] D. Bevers, N. Wagner, M. Bradke, *Int. J. Hydrogen Energy* **23** (1998) 57–63.

[55] S. Cha, W. Lee, *J. Electrochem. Soc.* **146** (1999) 4055–4060.

[56] A. Arico, P. Creti, P. Antonucci, J. Cho, H. Kim, V. Antonucci, *Electrochim. Acta* **43** (1998) 3719–3729.

[57] M. Williams, E. Begg, L. Bonville, H. Kunz, J. Fentom, *J. Electrochem. Soc.* **151** (2004) A1173–A1180.

[58] T. Zhou, H. Liu, *J. Power Sources* **161** (2006) 444–453.

[59] W.-K. Lee, C.-H. Ho, J. V. Zee, M. Murthy, *J. Power Sources* **84** (1999) 45–51.

[60] L. Jordan, A. Shukla, T. Bershing, N. Avery, B. Muddle, M. Forsyth, *J. Power Sources* **86** (2000) 250–254.

[61] Z. Qi, A. Kaufman, *J. Power Sources* **109** (2002) 38–46.

[62] C. Kong, D. Kim, H. Lee, Y. Shul, T. Lee, *J. Power Sources* **108** (2002) 185–191.

[63] E. Antolini, R. Passos, E. Ticcianelli, *J. Power Sources* **109** (2002) 477–482.

[64] A. Kumar, R. Reddy, *J. Power Sources* **114** (2003) 54–62.

[65] M. Mathias, J. Roth, J. Fleming, W. Lehnert, *Handbook of fuel cells - Fundamentals, technology and applications*, W. Vielstich, H. Gasteiger, A. Lamm (Eds.), Vol. 3, John Wiley & Sons, 2003, Ch. *Diffusion media materials and characterization*.

[66] D. Davies, P. Adcock, M. Turpin, S. Rowen, *J. Power Sources* **86** (2000) 237–242.

[67] D. Davies, P. Adcock, M. Turpin, S. Rowen, *J. Appl. Electrochem.* **30** (2000) 101–105.

[68] R. Makkus, A. Janssen, F. de Brujin, R. Mallant, *J. Power Sources* **86** (2000) 274–282.

[69] J. Wind, R. Späh, W. Kaiser, G. Böhm, *J. Power Sources* **105** (2002) 256–260.

[70] N. Cunningham, D. Guay, J. Dodelet, Y. Meng, A. Hill, A. Hay, *J. Electrochem. Soc.* **149** (2002) A905–A911.

[71] H. Wang, M. Sweikart, J. Turner, *J. Power Sources* **115** (2003) 243–251.

[72] J. Scholta, B. Rohland, V. Trapp, U. Focken, *J. Power Sources* **84** (1999) 231–234.

[73] T. Besmann, J. Klett, J. Henry, E. Lara-Curzio, *J. Electrochem. Soc.* **147** (2000) 4083–4086.

[74] E. Middelman, W. Kout, B. Vogelaar, J. Lenssen, E. D. Waal, *J. Power Sources* **118** (2003) 44–46.

[75] A. Schmitz, M. Tranitz, S. Wagner, R. Hahn, C. Hebling, *J. Power Sources* **118** (2003) 162–171.

[76] M. Wilson, Annular feed air breathing fuel cell stack, US Patent 5,514,486 (1996).

[77] J. Neutzler, M. Wilson, Annular feed air breathing fuel cell stack, US Patent 5,595,834 (1997).

[78] J. Meyers, H. Maynard, *J. Power Sources* **109** (2002) 76–88.

[79] J. Yu, P. Cheng, Z. Ma, B. Yi, *Electrochim. Acta* **48** (2003) 1537–1541.

[80] Q. Ye, T. Zhao, H. Yang, J. Prabhuram, *Electrochem. Solid-State Lett.* **8** (2005) A52–A54.

[81] A. Kulikovsky, H. Schmitz, K. Wippermann, J. Mergel, B. Fricke, T. Sanders, D. Sauer, *Electrochem. Commun.* **8** (2006) 754–760.

[82] M. McGovern, P. Waszczuk, A. Wieckowski, *Electrochim. Acta* **51** (2006) 1194–1198.

[83] R. J. Behm, Z. Jusys, *J. Power Sources* **154** (2006) 327–342.

[84] J.-T. Wang, S. Wasmus, R. Savinell, *J. Electrochem. Soc.* **143** (1996) 1233–1239.

[85] Q. Ye, T. Zhao, *J. Electrochem. Soc.* **152** (2005) A2238–A2245.

[86] K. D. Kreuer, S. Paddison, E. Spohr, M. Schuster, *Chem. Rev.* **104** (2004) 4637–4678.

[87] K. D. Kreuer, *Handbook of Fuel Cells - Fundamentals, Technology and Applications*, W. Vielstich, A. Lamm, H. Gasteiger (Eds.), Vol. 3, J. Wiley & Sons, Chichester, 2003, Ch. *Hydrocarbon membranes*, pp. 420–435.

[88] T. Fuller, J. Newman, *J. Electrochem. Soc.* **139** (1992) 1332–1337.

[89] X. Ren, T. Springler, T. A. Zawodzinski, S. Gottesfeld, *J. Electrochem. Soc.* **147** (2000) 466–474.

[90] X. Ren, T. E. Springler, S. Gottesfeld, *J. Electrochem. Soc.* **147** (2000) 92–98.

[91] T. Zawodzinski, C. Derouin, S. Radzinski, R. Sherman, V. Smith, T. Springer, S. Gottesfeld, *J. Electrochem. Soc.* **140** (1993) 1041–1047.

[92] T. Zawodzinski, J. Davey, J. Valerio, S. Gottesfeld, *Electrochim. Acta* **40** (1995) 297–302.

[93] M. Ise, K. D. Kreuer, J. Maier, *Solid State Ionics* **125** (1999) 213–223.

[94] K. Ley, R. Liu, C. Pu, Q. Fan, N. Leyarovska, C. Segre, E. Smotkin, *Electrochim. Acta* **144** (1997) 1543–1548.

[95] M. Hogarth, G. Hards, *Pt. Met. Rev.* **40** (1996) 150–159.

[96] A. Bard, L. Faulkner, *Electrochemical Methods: Fundamentals and Applications*, 2nd Edition, John Wiley & Sons, USA, 2001, Ch. 10, pp. 368–416.

[97] J. Selman, Y. Lin, *Electrochim. Acta* **38** (1993) 2063–2073.

[98] T. Springer, T. Zawodsinski, M. Wilson, S. Gottesfeld, *J. Electrochem. Soc.* **143** (1996) 587–599.

[99] B. Andreaus, A. McEnvoy, G. Scherer, *Electrochim. Acta* **47** (2002) 2223–2239.

[100] S. Slade, S. Campbell, T. Ralph, F. Walch, *J. Electrochem. Soc.* **149** (2002) A1556–A1564.

[101] D. Connolly, W. Gresham, Fluorocarbon Vinyl Ether Polymers, US Patent 3,282,875 (E.I. DuPont de Nemours and Company) (1966).

[102] R. Smith, Coextruded Multilayer Cation Exchange Membranes, US Patent 4,437,952 (E.I. DuPont de Nemours and Company) (1984).

[103] C. Preischl, P. Hedrich, A. Hahn, Continuous Method for Manufacturing a Laminated Electrolyte and Electrode Assembly, US Patent 6,291,091 (E.I. DuPont de Nemours and Company) (2001).

[104] D. Curtin, R. Lousenberg, T. Henry, P. Tangeman, M. Tisack, *J. Power Sources* **131** (2004) 41–48.

[105] K. Mauritz, R. Moore, *Chem. Rev.* **104** (2004) 4535–4585.

[106] M. Doyle, G. Rajendran, *Handbook of Fuel Cells - Fundamentals, Technology and Applications*, W. Vielstich, A. Lamm, H. Gasteiger (Eds.), Vol. 3, J. Wiley & Sons, Chichester, 2003, Ch. *Perfluorinated membranes*, pp. 351–395.

[107] W. Carl, B. Ezzel, Low equivalent weight sulfonic fluoropolymers, US Patent 4,940,525 (Dow Chemical Co.) (1990).

[108] B. Ezzel, W. Carl, Novel polymers having acid functionality, US Patent 4,330,654 (Dow Chemical Co.) (1980).

[109] B. Moore, C. Martin, *Macromolecules* **22** (1989) 3594–3599.

[110] M. Yamabe, H. Miyake, K. Arai, Fluoropolymer cationexchange membranes, Japanese Patent 5,228,588 (Asahi Glass Co.) (1977).

[111] H. Ukihashi, M. Yamabe, H. Miyake, *Progr. Polym. Sci.* **12** (1986) 229–270.

[112] Japanese Patent 5,761,339 (Asahi Glass Co.) (1977).

[113] H. Ukihashi, M. Yamabe, *Perfluorinated ionomer membranes*, A. Eisenberg, H. Yeager (Eds.), Vol. 17, American Chemical Society symposium series, Washington, 1982, Ch. *Perfluorocarboxylate polymer membranes*, pp. 427–451.

[114] M. Wakizoe, O. Velev, S. Srinivasan, *Electrochim. Acta* **40** (1995) 335–344.

[115] T. Zawodzinski, Jr., M. Neeman, L. Sillerud, S. Gottesfeld, *J. Phys. Chem.* **95** (15) (1991) 6040–6044.

[116] T. Kallio, M. Lundström, G. Sundholm, N. Walsby, F. Sundholm, *J. Appl. Electrochem.* **32** (2002) 11–18.

[117] X. Ren, T. Zawodzinski, F. Uribe, H. Dai, S. Gottesfeld, *Methanol Cross-Over in Direct Methanol Fuel Cells*, in: S. Gottesfeld, G. Halpert, A. Landgrebe (Eds.), *Proton Conducting Membrane Fuel Cells 1*, Vol. 95-23 of *The Electrochemical Society Proceedings Series*, Pennington, NJ, 1995.

[118] R. Jiang, D. Chu, *J. Electrochem. Soc.* **151** (1) (2004) A69–A76.

[119] E. Gülzow, T. Kaz, R. Reissner, H. Sander, L. Schilling, M. v. Bradke, *J. Power Sources* **105** (2002) 261–266.

[120] H. Dohle, J. Divisek, R. Jung, *J. Power Sources* **86** (1999) 469–477.

[121] H. Dohle, J. Divisek, J. Mergel, H. Oetjen, C. Zingler, D. Stolten, *J. Power Sources* **105** (2002) 274–282.

[122] B. Gurau, E. S. Smotkin, *J. Power Sources* **112** (2002) 339–352.

[123] S. Sandhu, R. Crowther, J. Fellner, *Electrochim. Acta* **50** (2005) 3985–3991.

[124] K. Scott, W. Taama, J. Cruickshank, *J. Appl. Electrochem.* **28** (1998) 289–297.

[125] J. Liu, T. Zhao, Z. Liang, R. Chen, *J. Power Sources* **153** (2006) 61–67.

[126] A. Chapiro, *Radiation Chemistry of Polymeric Systems*, Interscience Publishers, New York, 1962.

[127] D. Geymer, *In The Radiation Chemistry of Macromolecules*, M. Dole (Ed.), Vol. 1, Academic Press, 1972, Ch. 1.

[128] L. Mandelkern, *In The Radiation Chemistry of Macromolecules*, M. Dole (Ed.), Vol. 1, Academic Press, 1972, Ch. 13.

[129] B. Gupta, F. Büchi, G. Scherer, *J. Polym. Sci. Polym. Chem. Ed.* **32** (1994) 1931–1938.

[130] T. Kallio, K. Jokela, H. Ericson, R. Serimaa, G. Sundholm, P. Jacobsson, F. Sundholm, *J. Appl. Electrochem.* **33** (2003) 505–514.

[131] A. Aricò, V. Baglio, P. Cretì, A. D. Blasi, V. Antonucci, J. Brunea, A. Chapotot, A. Bozzi, J. Schoemans, *J. Power Sources* **123** (2003) 107–115.

[132] S. Hietala, S. Maunu, F. Sundholm, *J. Polym. Sci. Part B: Polymer Physics* **38** (2000) 3277–3284.

[133] K. Jokela, R. Serimaa, M. Torkkeli, F. Sundholm, T. Kallio, G. Sundholm, *J. Polym. Sci Part B: Polym. Phys.* **40** (2002) 1539–1555.

[134] S. Hietala, S. Holmberg, M. Karjalainen, J. Näsman, M. Paronen, R. Serimaa, F. Sundholm, S. Vahvaselkä, *J. Mater. Chem.* **7** (1997) 721–726.

[135] T. Lehtinen, G. Sundholm, S. Holmberg, F. Sundholm, P. Björnbom, M. Bursell, *Electrochim. Acta* **43** (1998) 1881–1890.

[136] N. Walsby, F. Sundholm, T. Kallio, G. Sundholm, *J. Polym. Sci. Part A: Polym. Chem.* **39** (2001) 3008–3017.

[137] N. Walsby, S. Hietala, S. Maunu, F. Sundholm, T. Kallio, G. Sundholm, *J. Appl. Polym. Sci.* **86** (2002) 33–42.

[138] T. Kallio, K. Kisko, K. Kontturi, R. Serimaa, F. Sundholm, G. Sundholm, *Fuel Cells* **4** (2004) 328–336.

[139] H. Ericson, T. Kallio, T. Lehtinen, B. Mattsson, G. Sundholm, F. Sundholm, P. Jacobsson, *J. Electrochem. Soc.* **149** (2002) A206–A211.

[140] F. Büchi, B. Gupta, O. Haas, G. Scherer, *Electrochim. Acta* **40** (1995) 345–353.

[141] H. Wang, G. Capuano, *J. Electrochem. Soc.* **145** (1998) 780–784.

[142] H. Brack, F. Büchi, J. Huslage, G. Scherer, *Recent Progress in the Development of the Radiation-Grafted PSI Membrane*, in: S. Gottesfeld, T. Fuller (Eds.), *Proceedings of the 2nd International Symposium on Proton Conducting Membrane Fuel Cells 2*, Vol. 98-27, The Electrochemical Society, Pennington, NJ, 1999.

[143] M. Schuster, K. Kreuer, H. Andersen, J. Maier, *Macromolecules* **40** (2007) 598–607.

[144] G. Scherer, E. Killer, D. Grman, *Int. J. Hydrogen Energy* **17** (1992) 115–123.

[145] M. Nasef, H. Saidi, M. Yarmo, *J. New Mat. Electrochem. Systems* **3** (2000) 309–317.

[146] X. Qiao, T.-S. Chunga, K. Pramoda, *J. Membr. Sci* **264** (2005) 176–189.

[147] J. Liu, H. Wang, S. Cheng, K.-Y. Chan, *J. Membr. Sci* **246** (2005) 95–101.

[148] Y. Kim, M. Hickner, L. Dong, B. Pivovar, J. McGrath, *J. Membr. Sci* **243** (2004) 317–326.

[149] A. Bard, L. Faulkner, *Electrochemical Methods: Fundamentals and Applications*, 2nd Edition, John Wiley & Sons, USA, 2001, Ch. 16, pp. 666–669.

[150] S. Ameniya, Z. Ding, J. Zhou, A. Bard, *J. Electroanal. Chem.* **483** (2000) 7–17.

[151] M. Mirkin, B. Horrocks, *Anal. Chim. Acta* **406** (2000) 119–146.

[152] T. Kallio, C. Slevin, G. Sundholm, P. Holmlund, K. Kontturi, *Electrochem. Commun.* **5** (2003) 561–565.

[153] A. Bard, F.-R. Fan, M. Mirkin, *Scanning electrochemical microscopy*, A. Bard (Ed.), Vol. 18, Marcel Dekker, New York, 1994, Ch. *Electroanalytical Chemistry*, pp. 255–258.

[154] T. Zawodzinski, S. Gottesfeld, S. Shoichet, T. McCarthy, *J. Appl. Electrochem.* **23** (1993) 86–88.

[155] N. Walsby, M. Paronen, J. Juhanoja, F. Sundholm, *J. Appl. Polym. Sci.* **81** (2001) 1572–1580.

[156] R. Yeo, *Polymer* **21** (1980) 432–435.

[157] D. Nandan, H. Mohan, R. Iyer, *J. Membr. Sci.* **71** (1992) 69–80.

[158] C. Gates, J. Newman, *AIChE J.* **46** (2000) 2076–2085.

[159] A. Geiger, J. Newman, J. Prausnitz, *AIChE J.* **47** (2001) 445–452.

[160] R. Yeo, C.-H. Cheng, *J. Appl. Polym. Sci.* **32** (1986) 5733–5741.

[161] G. Gebel, P. Aldebert, M. Pineri, *Polymer* **34** (1993) 333–339.

[162] N. Munichandraiah, K. McGrath, G. Prakash, R. Aniszfeld, G. Olah, *J. Power Sources* **117** (2003) 98–101.

[163] E. Cussler, *Diffusion Mass Transfers in Fluid Systems*, 2nd Edition, Cambridge University Press, New York, 1997.

[164] V. Barrágan, C. Ruiz-Bauzá, J. Villaluenga, B. Seoane, *J. Power Sources* **130** (2004) 22–29.

[165] T. Schaffer, V. Hacker, T. Hejze, T. Tschinder, J. Besenhard, *J. Power Sources* **145** (2005) 188–198.

[166] X. Ren, W. Henderson, S. Gottesfeld, *J. Electrochem. Soc.* **144** (1997) L267–L270.

[167] X. Ren, S. Gottesfeld, *J. Electrochem. Soc.* **148** (2001) A87–A93.

[168] S. Cleghorn, C. Derouin, M. Wilson, S. Gottesfeld, *J. Appl. Electrochem.* **28** (1998) 663–672.

[169] J. Stumper, S. Campbell, D. Wilkinson, M. Johnson, M. Davis, *Electrochim. Acta* **43** (1998) 3773–3783.

[170] C. Wieser, A. Helmbold, E. Gülzow, *J. Appl. Electrochem.* **30** (2000) 803–807.

[171] M. Noponen, T. Mennola, M. Mikkola, T. Hottinen, P. Lund, *J. Power Sources* **106** (2002) 304–312.

[172] M. Noponen, T. Hottinen, T. Mennola, M. Mikkola, P. Lund, *J. Appl. Electrochem.* **32** (2002) 1081–1089.

[173] T. Hottinen, M. Noponen, T. Mennola, O. Himanen, M. Mikkola, P. Lund, *J. Appl. Electrochem.* **33** (2003) 265–271.

[174] M. Noponen, J. Ihonen, A. Lundblad, G. Lindbergh, *J. Appl. Electrochem.* **34** (2004) 255–262.

[175] Z. Liu, Z. Mao, B. Wu, L. Wang, V. Schmidt, *J. Power Sources* **141** (2005) 205–210.

[176] X.-G. Yang, N. Burke, C.-Y. Wang, K. Tajiri, K. Shinohara, *J. Electrochem. Soc.* **4** (2005) A759–A766.

[177] R. Eckl, R. Grinzinger, W. Lehnert, *J. Power Sources* **154** (2006) 171–179.

[178] R. Liu, E. Smotkin, *J. Electroanal. Chem.* **535** (2002) 49–55.

[179] M. Mench, Q. Dong, C. Wang, *J. Power Sources* **124** (2003) 90–98.

[180] A. Geiger, R. Eckl, A. Wokaun, G. Scherer, *J. Electrochem. Soc.* **151** (2004) A394–A398.

[181] D. Brett, S. Atkins, N. Brandon, V. Vesovic, N. Vasileiadis, A. Kucernak, *Electrochem. Solid-State Lett.* **6** (2003) A63–A66.

[182] G. Bender, T. Zawodzinski, *Spatial distribution of the CO transient response of a PEFC*, in: *Proceedings - Electrochemical Society*, Vol. 2002-31 (Proton Conducting Membrane Fuel Cells III), Electrochemical Society, Los Alamos National Laboratory, Los Alamos, NM, USA, 2005, pp. 212–219.

[183] J. Villaluenga, B. Seoane, V. Barrágan, C. Ruiz-Bauzá, *J. Colloid Interface Sci.* **268** (2003) 476–481.

[184] T. Schaffer, T. Tschinder, V. Hacker, J. Besenhard, *J. Power Sources* **153** (2006) 210–216.

[185] J. Villaluenga, B. Seoane, V. Barrágan, C. Ruiz-Bauzá, *J. Membr. Sci* **274** (2006) 116–122.

[186] V. Silva, A. Mendes, L. Madeira, S. Nunes, *J. Membr. Sci* **276** (2006) 126–134.

[187] C.-Y. Wang, *Chem. Rev.* **104** (2004) 4727–4766.

[188] A. Weber, J. Newman, *Chem. Rev.* **104** (2004) 4679–4726.

[189] K. Yao, K. Karan, K. McAuley, P. Oosthuizen, B. Peppley, T. Xie, *Fuel Cells* **4** (2004) 3–29.

[190] A. Kulikovsky, *Electrochem. Commun.* **4** (2002) 939–946.

[191] C.-H. Chen, T.-K. Yeh, *J. Power Sources* **160** (2006) 1131–1141.

[192] J. Rice, A. Faghri, *Int. J. Heat Mass Transfer* **49** (2006) 4804–4820.

[193] S. Zhou, T. Schultz, M. Peglow, K. Sundmacher, *Phys. Chem. Chem. Phys.* **3** (2001) 347–355.

[194] Z. Wang, C. Wang, *J. Electrochem. Soc.* **150** (2003) A508–A519.

[195] V. Danilov, J. Lim, I. Moon, H. Chang, *J. Power Sources* **162** (2006) 992–1002.

[196] R. Chen, T. Zhao, *J. Power Sources* **152** (2005) 122–130.

[197] W. Yang, T. Zhao, *Electrochim. Acta* **52** (2007) 6125–6140.

[198] E. Kjeang, J. Goldak, M. Golriz, J. Gu, D. James, K. Kordesch, *J. Power Sources* **153** (2006) 89–99.

[199] W. Liu, C.-Y. Wang, *J. Power Sources* **164** (2007) 561–566.

[200] J. Ge, H. Liu, *J. Power Sources* **160** (2006) 413–421.

[201] H. Ju, C.-Y. Wang, *J. Electrochem. Soc.* **151** (2004) A1954–A1960.

[202] J. Norlund, G. Lindbergh, *J. Electrochem. Soc.* **149** (2002) A1107–A1113.

[203] K. Jeng, C. Chen, *J. Power Sources* **112** (2002) 367–375.

[204] T. Mennola, M. Noponen, M. Aroniemi, T. Hottinen, M. Mikkola, O. Himanen, P. Lund, *J. Appl. Electrochem.* **33** (2003) 979–987.

[205] J. Larminie, A. Dicks, *Fuel Cell Systems Explained*, 2nd Edition, John Wiley & Sons, West Sussex, 2003.

[206] S. Sangribsub, P. Tangboriboonrat, T. Pith, G. Decher, *Polym. Bull.* **53** (2005) 425–434.

[207] R. Jisr, H. Rmaile, J. Schlenoff, *Angewandte Chem. Int.* **44** (2005) 782–785.

[208] H. Brack, M. Wyler, G. Peter, G. Scherer, *J. Membr. Sci* **214** (2003) 1–19.

[209] D. Ramdutt, C. Charles, J. Hudspeth, B. Ladewig, T. Gengenbach, R. Boswell, A. Dicks, P. Brault, *J. Power Sources* **165** (2007) 41–48.

[210] S. de Almeida, Y. Kawano, *J. Therm. Anal. Cal.* **58** (1999) 569–577.

[211] Y. Sone, P. Ekdunge, D. Simonsson, *J. Electrochem. Soc.* **143** (1996) 1254–1259.

[212] F. Bauer, S. Denneler, M. Willert-Porada, *J. Polym. Sci. B: Polym. Phys.* **43** (2005) 786–795.

[213] E. Skou, P. Kauranen, J. Hentschel, *Solid State Ionics* **97** (1997) 333–337.

[214] V. Freger, E. Korin, J. Wisniak, E. Korngold, M. Ise, K. Kreuer, *J. Membr. Sci.* **160** (1999) 213–224.

[215] K. Scott, W. Taama, P. Argyropoulos, *J. Membr. Sci.* **171** (2000) 119–130.

[216] T. Hatanaka, N. Hasegawa, A. Kamiya, M. Kawasumi, Y. Morimoto, K. Kawahara, *Fuel* **81** (2002) 2173–2176.

[217] H. Dohle, J. Mergel, D. Stolten, *J. Power Sources* **111** (2002) 268–282.

ISBN 978-951-22-8980-6
ISBN 978-951-22-8981-3 (PDF)
ISSN 1795-2239
ISSN 1795-4584 (PDF)